MSUCP-27

MICHIGAN STATE UNIVERSITY

CYCLOTRON PROJECT

Cyclotron Ion Starting Times In The Second Harmonic Accelerating Mode*

H. B. White, Jr.

Department of Physics - Cyclotron Laboratory

East Lansing, Michigan

July, 1974

*This work was partially supported by the National Science Foundation

ABSTRACT

CYCLOTRON ION STARTING TIMES IN THE SECOND HARMONIC ACCELERATING MODE

By

Herman Brenner White, Jr.

The analysis of orbit histories of the Michigan State University Isochronous Cyclotron by computer calculations is complicated in the central region because of the strong electric forces. A study was begun to improve the second harmonic operation utilizing the orbit code CYCLONE and measured electric fields in the central region. Presented here is the experimental analysis of the orbit calculations in terms of the correlation between predicted beam positions by CYCLONE and experimentally determined positions by foil burns. The data is presented graphically to exhibit the close fit or deviation of the data with various runs of the computer code, both for previously used fields and for the new fields. Finally the work is extended to help predict the optimum starting time and also therefore, the starting phase of the particle beam.

TABLE OF CONTENTS

Note Added in Proof:

An angular alignment error between the puller gap and the ion source face has recently been observed; this error presumably existed at the time of the foil burn runs described herein. The ion source face was intended to be parallel to the face of the puller; telescopic measurements showed a deviation due to the calibration errors as shown in the sketch (viewed from the top):

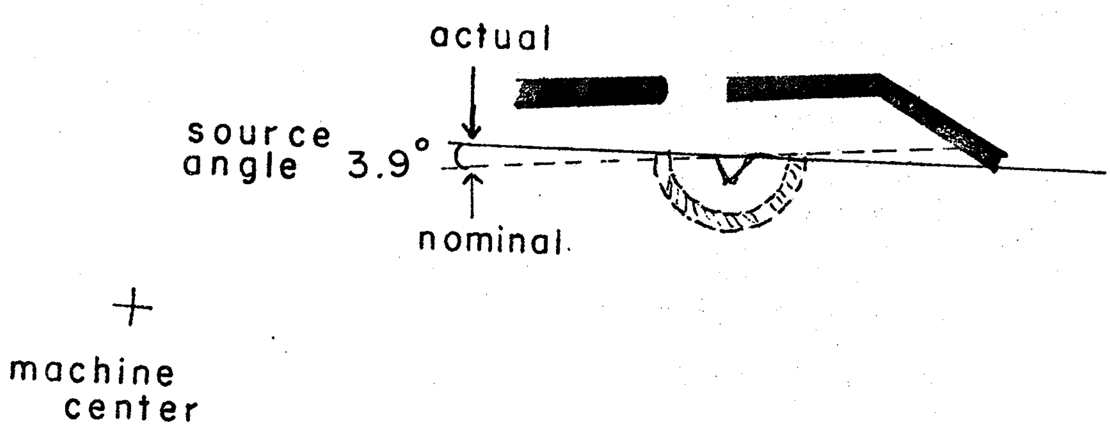

The conclusions of this study are presumably slightly affected by this error; results should be interpreted accordingly.

LIST OF TABLES

Table Page

LIST OF FIGURES

Figure Page

1. FORWARD

It has been often said lately, that most scientific work reflects very little of the human element behind it. While the explanation of the work might very well be directed to the specialist in the field, the reasons for doing it and the research development behind it surely can be for the general reader. Luis Alvorez has pointed out that, "We should welcome. . .publications in which physicists tell us not only what they did, but why they did it, as well."[1] Therefore with this spirit and in this brief forward I should like to relate how this topic came about.

After having been involved with experimental modern (nuclear) physics as an undergraduate, I began work in trace elements here at Michigan State University using nuclear scattering techniques. This experience amply whetted my appetite for experimental work, and as a result I ventured off to other laboratories during the summer to increase my effectiveness in nuclear physics. While studying the $^{208}Pb(\alpha,p)$ reaction at Argonne National Laboratory, I made frequent trips to the National Accelerator Laboratory at Batavia and it became apparent to me that a large part of our study of nuclear and particle physics could be found in the study of the accelerators themselves. One could say understanding what the experiment does depends on understanding how the equipment works. In the following years I concentrated on accelerators and in particular the MSU Cyclotron. Prof. Blosser presented many questions about the machine (and answers I might add). The question of what happens to acceleration in the "Central Region" of the machine was one question some effort had been put into before. The central region being the area of the beginning history of the particle's acceleration. In this machine often times first harmonic operation has tended to be the best. Therefore, by studying this central region we felt that second harmonic acceleration could be improved. After spending some time working on the CERN Synchro-Cyclotron, in magnetic measurements and particle detection, I began making electrical field measurements on the central region of the MSU Cyclotron. One important, and it turns out, very fundamental question arose: "How well can we predict, using these measurements, orbit properties of the accelerated beams in the Cyclotron?" Moreso, how accurate are our orbit calculations for second harmonic operation?

Preliminary to the final computations of the orbit properties, a study was necessary after the measurements to verify that the orbit calculations did indeed correspond to what actually happens inside the cyclotron machine. Therefore, it was necessary to correlate the calculated particle properties with observed results which is the intent of this study.

2. INTRODUCTION

The Michigan State University Sector Focused Cyclotron is a multi-particle, variable energy machine with a maximum proton energy of 56 MeV. The RF-system consist of two 138° dees and a 42° dummy dee which can be operated in either push-pull or push-push modes, over a frequency range of approximately 13.5 to 22 mega-cycles.[2]

The difficult analysis of orbit histories has in recent years been made easier by the use of the computer. The MSU Cyclotron Laboratory utilizes the Xerox Sigma-7 computer with which all the calculations for this study were made. The initial orbits calculated are crucial in determining the properties of the final extracted beam, such that the central region of the machine becomes of key importance. The complexity of the central region problem can be in part due to the interaction of particles with the magnetic forces, electrical forces, and space charge forces. Typically to study these forces one generally concentrates on accurately measuring the fields involved. Much attention is placed on the magnetic field outside of the central region,[3,4,5] since the particles are affected by magnetic forces here a longer period of time. That is, they are outside of the accelerating gaps longer being bent by the magnetic field than inside the gaps being dominated by the electrical accelerating forces.

The electric field of the dees and the particular electric field configuration of the source-puller system becomes very important in understanding the initial orbit properties of the beam. Previous studies[6,7] have been done which discuss the central region geometry and orbit properties for previous electrical field measurements. Even though the theoretical calculations for particle trajectories and properties are based on physical laws, we still use these measurements as observed input data, to predict future behavior.

Since the last detail measurements of the electric field in the central region, some physical structure changes have occurred which could change the orbit properties of the cyclotron beam. To study these orbits it was necessary to make detailed measurements of the central region electric fields for the new geometry. Other measurements were made for the N=1 mode.[8] Thus this study presents calculations for the N=2 mode to experimentally verify second harmonic orbit calculations.

3. PROCEDURE

3.1 Electrolytic Tank Measurement

The central region electric field measurements were done using an automatic electrolytic tank facility.[9] The electric fields obtained were measurements of a rectangular grid of potential values in a two-dimensional array of points, ten square inches in size. The tank is characterized by a motor driven probe and the voltage of each point of the rectangular grid is automatically balanced to ground by a self-balancing bridge and punched on an IBM card. The scale is 1:1 for the actual machine.

The tank geometry is a scale model of the central region of the Cyclotron machine as shown in Figure 1. This geometry corresponds to the N=1 mode (push-pull) of acceleration with 134°-dees. The electrolyte used was doubly-deionized water, with the water-level in the tank at just above the top of the center electrode at the source position, to correspond to the median plane in the actual machine. A braking system was used on the tank's longitudinal movement to increase the amount of time for the bridge circuit to balance. This provides for a more accurate position of the probe at the time the voltage at that position is measured. Also oxidation and erosion of the copper surfaces

FIGURE 1.--Electrolytic tank model of the central region with the source and puller in the N=1 configuration. This structure shows one side of the median plane with the electrodes at the center defining the water level. Scale is 1:1.

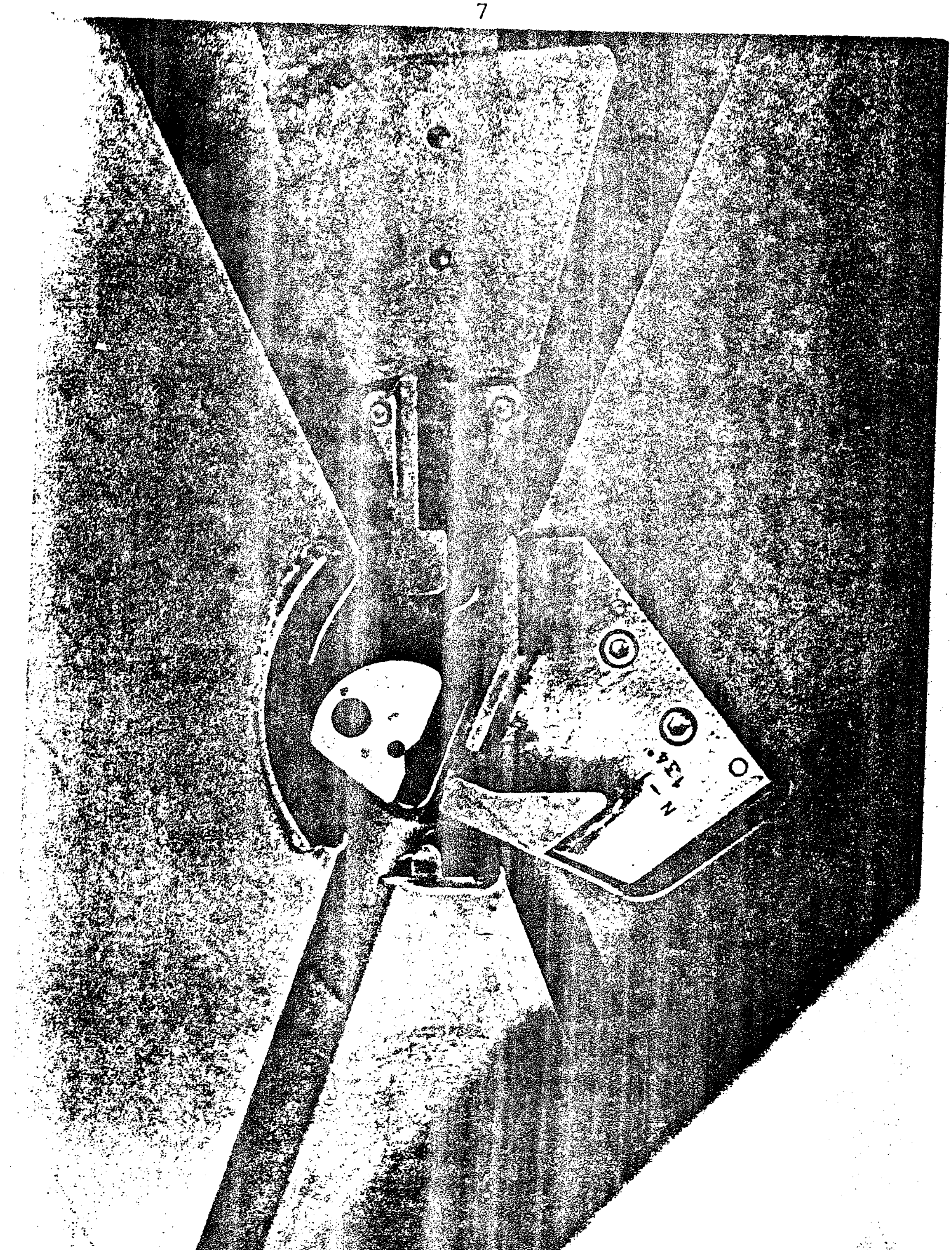

Figure 1

were reduced by cleaning and the use of a dust cover. The cover also prevented conductive materials from contacting the water surface, as well as reducing motion of the water by air currents.

Another improvement was the larger size of the data grid, making possible more accurate calculations further out from the machine center. Consistant accuracy of ±0.5% was common in this measurement. All electric field data for orbit studies are stored in the laboratory computer library and coded for identification with a heading and a parameter list that gives all pertinent information concerning the potential grid that follows. The data (100x100 data points; large electric field) was first checked by plotting it with the computer in the form of an equipotential contour-map as shown in Figure 2. The utility of this procedure was to check that the geometry suggested was in fact reproduced in the gathered data. Also accuracy can be considered if all the equipotential contours are continuous and do not overlap, as they should provide analytical solutions to Laplace's equations for this complex geometry. The equipotential contours are plotted for potential values representing 2% of the total range of potentials, that is from 2% to 98%. These contours can be compared with the N=2 contours from a previous measurement.

It should be noted that the electrolytic tank geometry in this field study is for the N=1 harmonic mode, but the

FIGURE 2.--Equipotential contour map for 134° dees from electrolytic tank data, in the N=2, push-push mode. The field coded 2.138.2A is the new field rotated by 45°. The old field, coded 204.5-L, contour map indicates the N=2 source to puller position with the puller recessed into the dee. In both cases these represent 2% contours of the total potential.

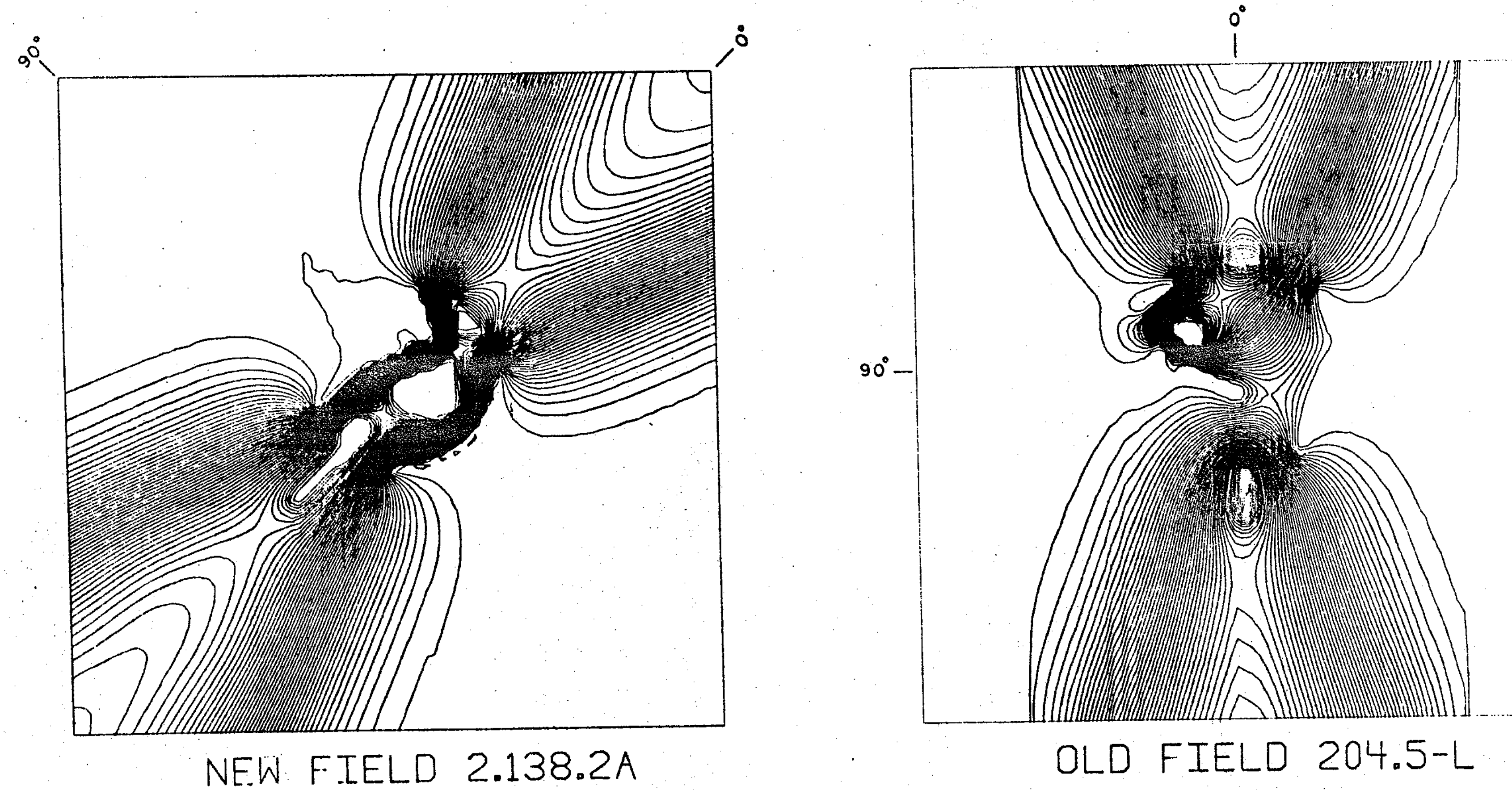

Figure 2

tank was run in the N=2 harmonic mode. The computer program used for these orbit calculations considers the forces due to the large electric field to not be included until the particle's angular position on the initial turn is greater than 90 degrees.[10] The change in the position of the source and puller, however, is due to the phase dependence of the beam on the initial turns. That is, there is some starting phase (ϕ_o) for which the acceleration is a maximum, for which:

$$\int_0^{E_{max}} \sin \phi \; (E) dE = 0.$$

Since the magnetic field cone in the machine center shifts the particle's phase by approximately 21°, lengthening the first half turn compensates for this phase shift.[11] This puts the initial particle phase with respect to the rf near zero and results in the largest energy gain for the acceleration. Therefore, if the shift due to particles leaving the source on the peak of the rf cycle is approximately 21°, then recessing the source and puller into the dee by this amount will compensate for this phase shift. On the other hand, in the computer code the assumption is made that the particle only drifts after the source to puller field until it reaches 90° where the large electric field picks it up.

For this measurement the two dees have the same potential with one dummy dee grounded and the other having a potential 10% of the dees.

3.2 Source to Puller Field Measurements

The accuracy of the fields are important for accurate and reliable particle orbit calculations to be done later. For this reason special attention was placed on what is known as the source to puller region field. In this region the electric field is changing very rapidly and the accuracy of the electrolytic tank is not sufficient (with the total central geometry) to give very useful data in this critical region of the electrode geometry. This region characterizes the beginning motion of the ions to be accelerated. Since the magnetic field is comparatively very weak here, the electric field is the major focusing mechanism in the source to puller region.

The electrolytic tank was set to measure data at .1 inch resolution. Thus with the source to puller region of interest being approximately .50 square inches (on this scale), one would not get a reasonable resolution of the field in this area. To overcome this problem, a 20:1 scale drawing of the source and puller were made on conduction papers in much the same way as the 3 dimensional tank geometry. Electrodes were fixed to the paper by G. C. Electronics Silver conducting paint out-lining the perimeter of the electrode geometry. Using the Fluke 8200A Digital Voltmeter, a 15 inch by 20 inch grid with 0.025 inch spacing, of voltages was taken to constitute this smaller electric field. This geometry's equipotential contour map is shown in Figure 3. For comparison the old electric field is also presented (1.06.7-S).

Definite improvements can be noted in these small field measurements. The larger scale made it possible to get more accurate data at the source slit. As can be seen, some physical changes were made from the previous 30° recessed source slit, mainly its position with respect to the puller gap. Previously, values at the source slit had to be interpolated to yield a continuous field because the number of data points in the slit itself was limited by the scale used. Therefore with a larger scale it was possible to obtain the necessary data points needed with a minimal use of interpolation.

3.3 General Outline of Foil Burning Technique

Predicted positions of the beam path can only be verified by physical measurements of the beam positions. To make these measurements the technique of foil-burning was employed.

A mesh of stainless steel, .0045 inches thick with 200 mesh squares per square inch, and 5.0 square inches in size was placed between the plane of the dees in the path of the accelerating beam. Foil holders were adapted to fit the current physical dimensions of the central region.

FIGURE 3.--Equipotential contour map for the source to puller electric field. Both 2% contours and the electric field configuration clearly shows the geometric change in the position of the source relative to the puller gap. Field 1.06.9-S was gathered on a 20:1 potential grid; the old field on a 10:1 grid. Both plotted 10:1 as shown, for N=2.

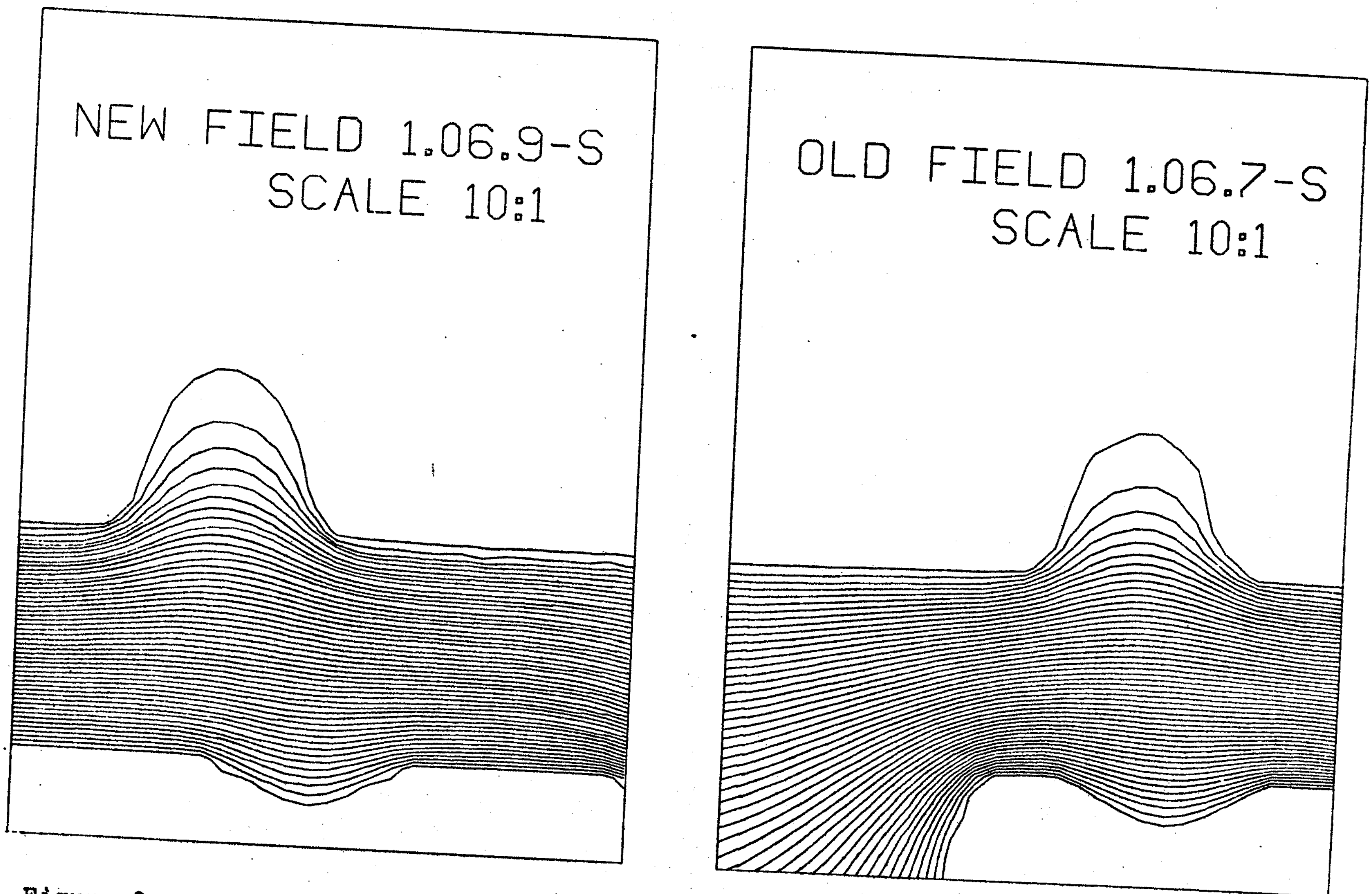

Figure 3

The foils were placed at 0°, 90°, and 270°. A differential probe trace was used in the 180° position, to define the beam path.

The machine was first set to yield a 24 MeV deuteron beam, and a complete differential probe trace turn pattern was done to get the total number of turns for the accelerated beam. This information is used to determine the approximate dee voltage. A vacuum break in the main chamber is necessary to place the foils, after which it is only necessary to restart the machine leaving the controls as they were, so that the parameters for the machine remain a constant. For this study centering coils were not used so that the magnetic field data would be in its simplest form for calculation.

As the beams impinges on the foil, the area of the beam heats the foil and eventually burns a hole at that radius, leaving the edges glowing as can be seen from Figures 4, 5 and 6. The back of the copper foil holders acts as a beam stop so the particles don't accelerate further than the central region of interest which for this study was six turns. In measuring the 180° beam position, one limitation was power dissipation on the beam probe. After burning the foils we lowered the intensity of the beam to within a safe region. The power is given by:

$$P(\text{watts}) = E(\text{MeV}) \times i\ (\mu\ \text{amps})/Z$$

For our study at less than 10 inches radius with a beam current of 300 μA we dissipated approximately 7×10^3 watts

FIGURE 4.--Foil holes near the 0° symmetry line of the machines. The glow comes from the beam burning the foils at 90° on the right and 270° on the left, for the 2nd run, of 24 MeV deuterons.

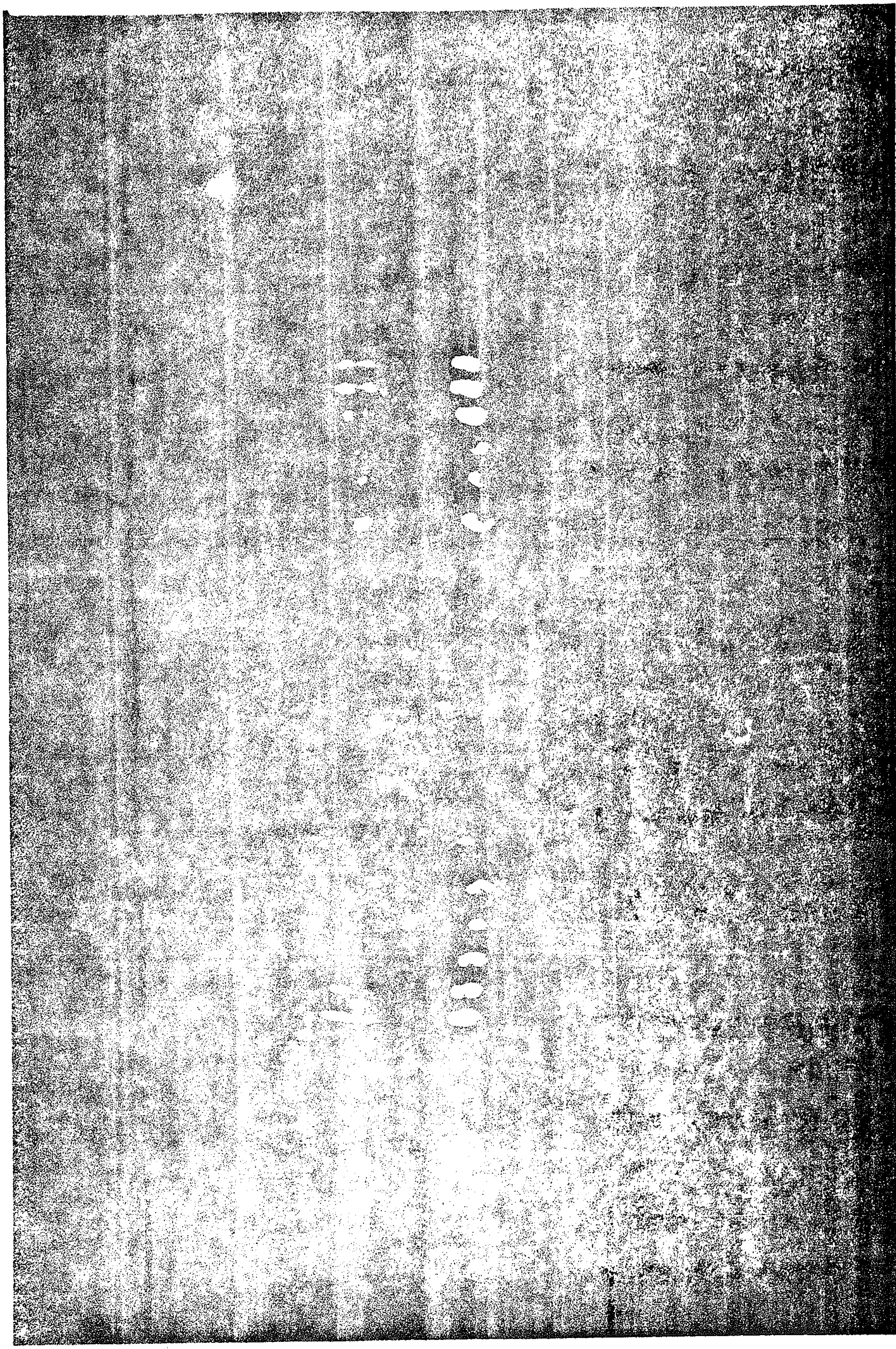

Figure 4

FIGURE 5.--Holes glowing along deflector angle. Position indicated by arrow in Figure 10. Photo shows first 5 turns at 0° and 4 turns at 270°, (1st turns at 270° blocked from view by foil holder at 0°).

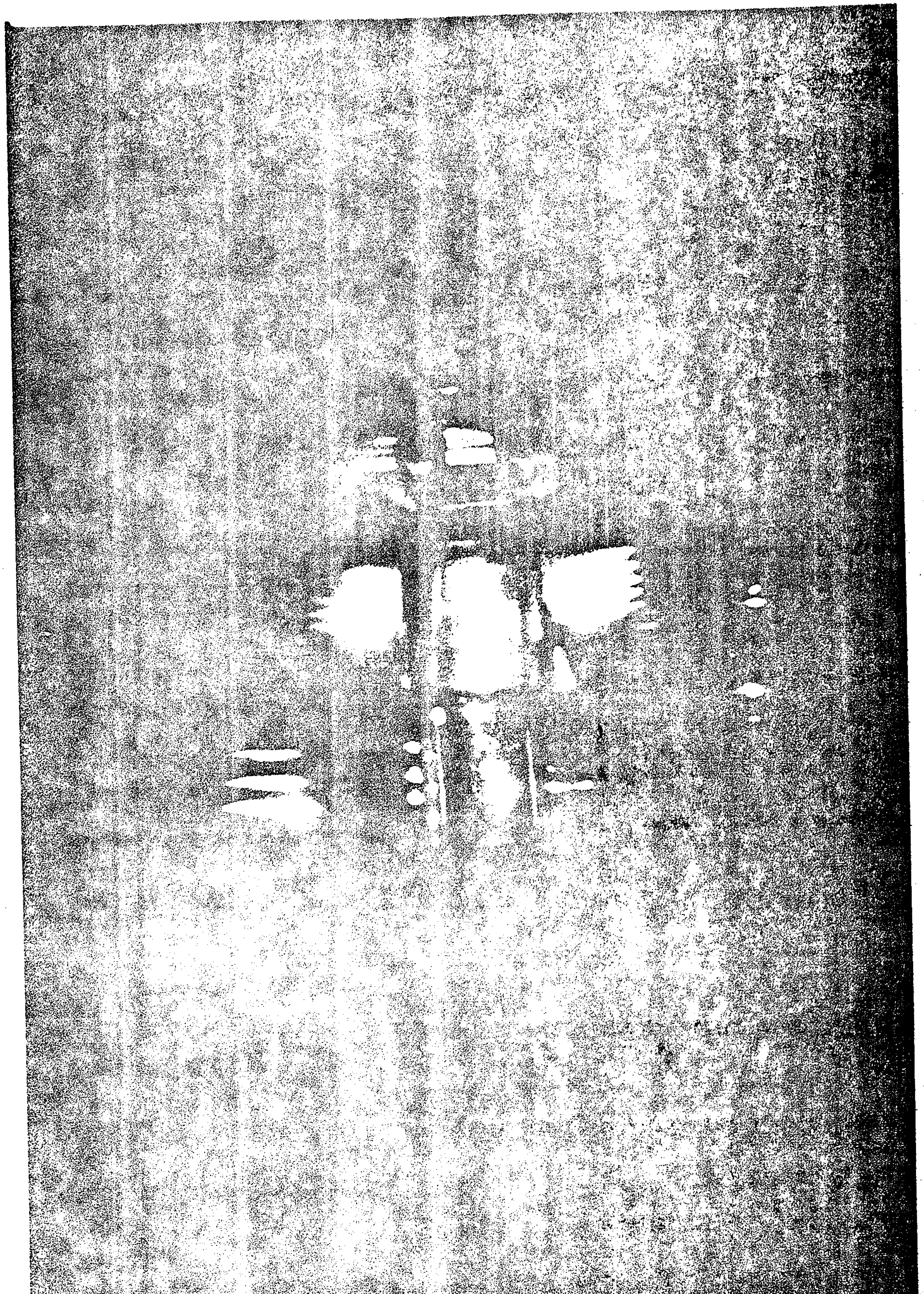

Figure 5

FIGURE 6.--Foil hole along detector angle as in Figure 5, showing the first turn on 0° just as the beam is about to burn through. Photo of 2nd run. Position of view indicated by arrow in Figure 10.

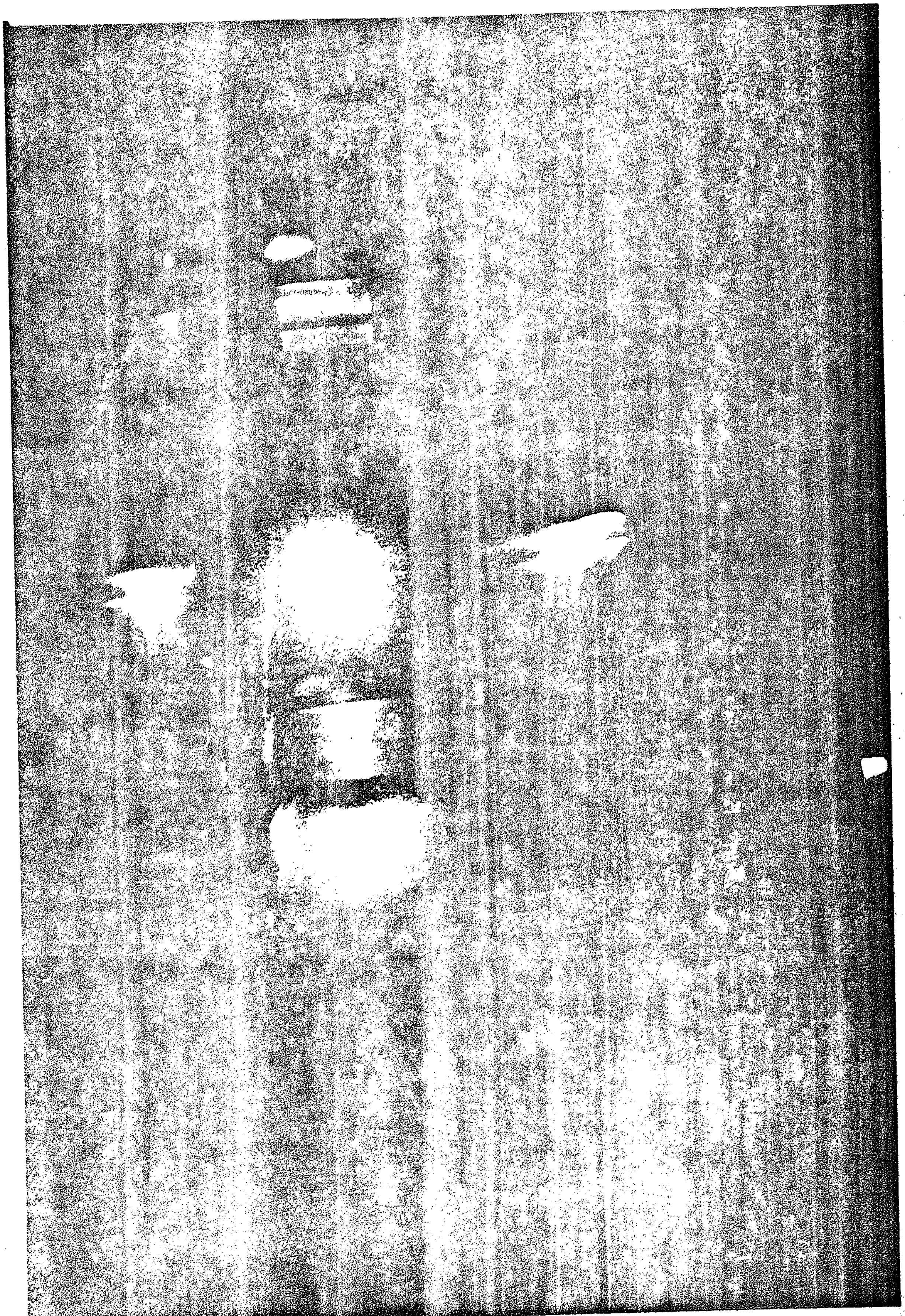

Figure 6

FIGURE 7.--Differential probe trace patterns. The probe is positioned at 180° and (a) shows the data at this angle giving the inner and outer turn radii. A full turn pattern with no centering coils in (b).

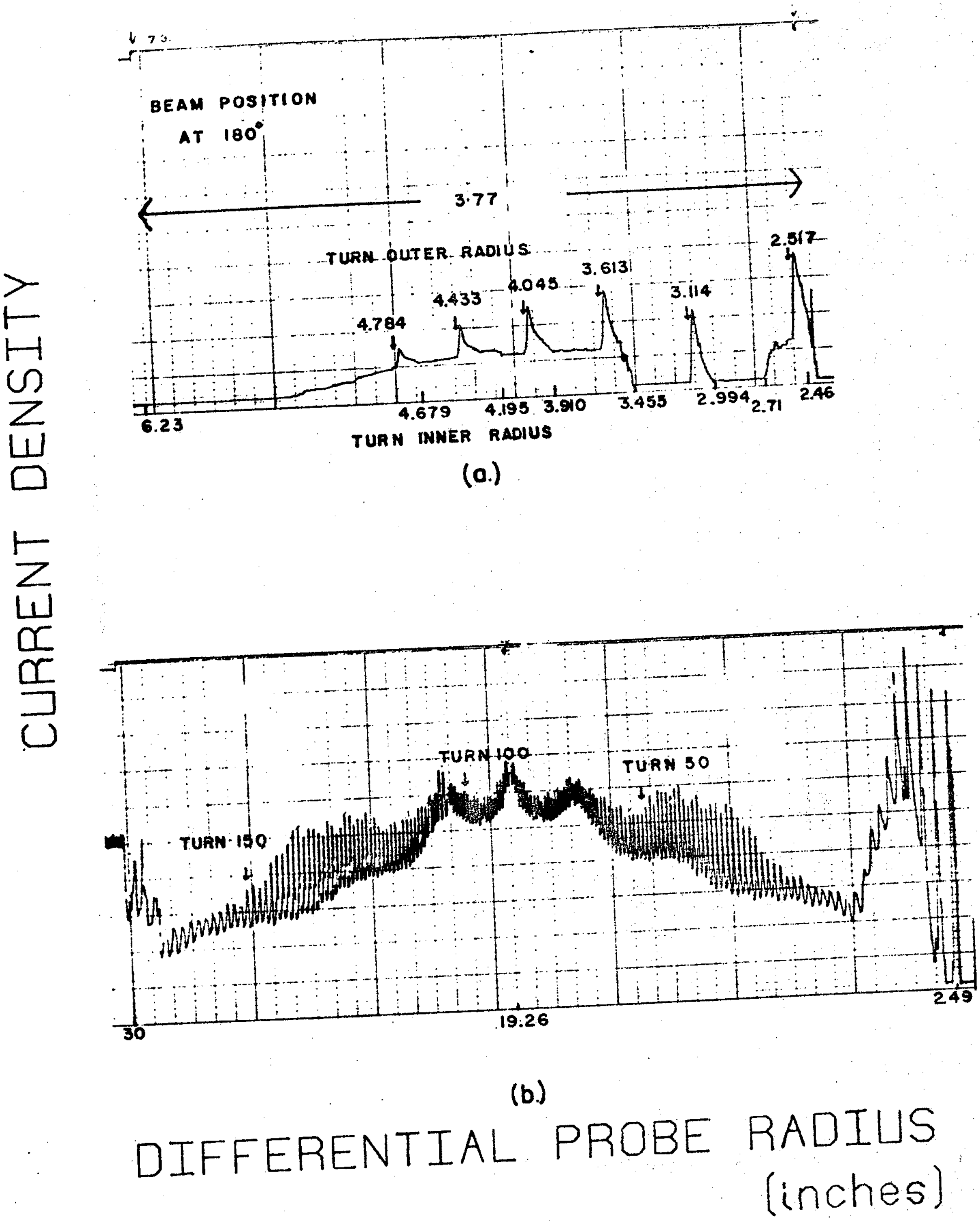
CURRENT DENSITY
BEAM POSITION
AT 180°
3.77
TURN OUTER RADIUS
4.784
4.433
4.045
3.613
3.114
2.517
6.23
4.679
4.195
3.910
3.455
2.994
2.71
2.46
TURN INNER RADIUS
(a.)
TURN 150
TURN 100
TURN 50
30
19.26
2.49
(b.)
DIFFERENTIAL PROBE RADIUS
(inches)

Figure 7

machine center was used as a radius vector. The position of each hole therefore was measured as a change in angle from the reference position (0°), with an assumed constant radius. Table II gives the radius of the holes, in the first run, with relation to the measured angles using the transit compass method. To check the data initially, the separation between each hole was compared to a vernier caliper measurement of the separation using the foil alone. Table II shows that this difference is as much as 0.1 inches. This method was abandoned because of these errors as well as other errors from slight motion of the transit. The data is also corrected on the south dee (90° position) for radial shift of the dees by .0625 inches due to the vacuum.

However, it was observed that each foil holder had been constructed with certain dimensions and alignment pins so they could be placed precisely, from the current cyclotron mechanical drawings. This method was pursued such that the position of the holders were known well with relation to the machine and therefore the 270°, 0°, and 90° data were measured with relation to the foil holders themselves. This arrangement is shown in Figure 8. The front edge of the copper holders was used as the reference point.

Table III and Table IV give the turn number, radius data, and angles for similar runs of 24 MeV deuterons, where the measurements were all done with respect to the foil holders. In Table IV, the 180° data is taken from the

TABLE II.--Foil hole radii at 90° and 270° for the first run determined by the transit compass measurements and calculations. Angle accuracy to 1 minute. The trigonometric radius vector used was 114.937 inches±.001 inch. South dee (90° data) corrected for radial displacement due to vacuum. Measurements relate to distance from machine center.

	Position (degrees)	Radius (inches)	Calculated Separation (inches)	Measured Separation (inches)
90°	1°12'=1.2°	2.346	> .769	.623
	1°35'=1.583°	3.115	> .569	.524
	1°52'=1.867°	3.684	> .536	.415
	2°08'=2.133°	4.220	> .468	.371
	2°22'=2.367°	4.088	> .436	.355
	2°35'=2.583°	5.124		
270°	1°18'=1.3°	2.608	> .636	.734
	1°37'=1.617°	3.244	> .502	.612
	1°52'=1.867°	3.746	> .435	.514
	2°5' =2.083°	4.181	> .368	.469
	2°16'=2.267°	4.549	> .469	.408
	2°30'=2.50°	5.018		

FIGURE 8.--The foil holders and their dimensions relative to the center of the Cyclotron at 0°, 90°, and 270°. The measurements are accurate to .001 inch. Note 90° and 270° are presented laying flat on the side viewed from the top.

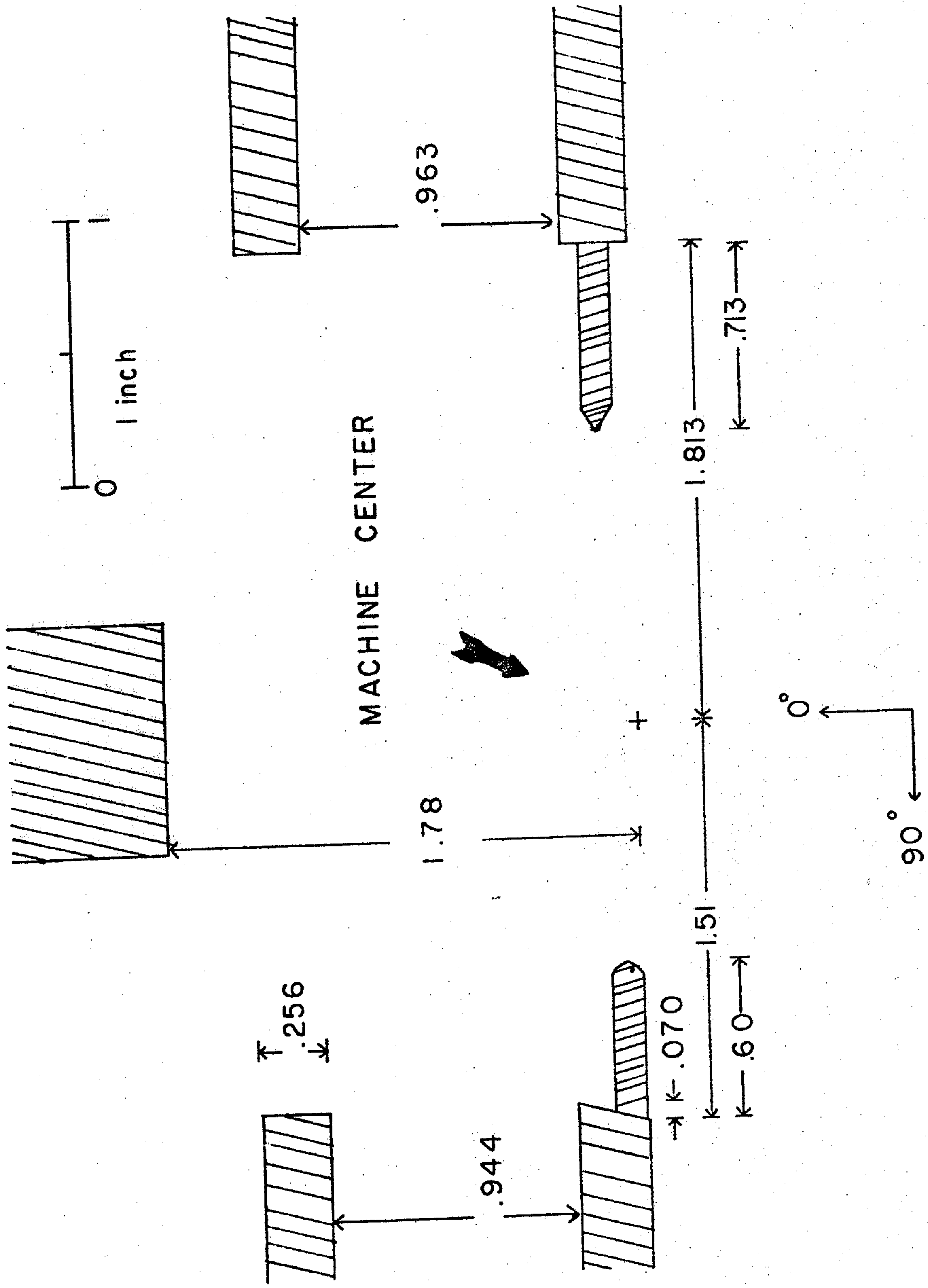

Figure 8

TABLE III.--Hole measurements data for run 1 (24 MeV deuterons) obtained using the foil holders and mechanical drawing as references. Positions corresponds to geometry in Figure 8. Raw data from foil holders alone and final radii to an accuracy of .001 inch. No data shown at 180°.

Turn #	0° Raw data	0° Radius	90° Raw data	90° Radius	270° Raw data	270° Radius
0	-	-	-	-	-	-
	-	-	-	-	.263	2.076
1	.212	1.992	.432	1.942	.954	2.767
	.312	2.092	.552	2.062	1.137	2.950
2	1.029	2.809	1.183	2.693	1.576	3.389
	1.127	2.907	1.316	2.826	1.766	3.579
3	1.636	3.416	1.857	3.367	2.092	3.905
	1.775	3.555	1.943	3.453	2.251	4.064
4	2.163	3.943	2.362	3.872	2.530	4.343
	2.291	4.071	2.462	3.972	2.693	4.506
5	2.590	4.370	2.844	4.354	2.949	4.762
	2.722	4.502	2.918	4.428	3.097	4.910
6	3.016	4.796	3.265	4.775	3.354	5.167
	3.112	4.892	3.337	4.847	3.461	5.274
7	3.441	5.221				
	3.492	5.272				

TABLE IV.--Radii for run-2 using the foil holders and mechanical drawings as reference. Data at 0°, 90°, 180°, and 270° indicated. Raw data from foil holders alone and final radii all in inches (±.001 inch).

Turn #	0° Raw data	0° Radius	90° Raw data	90° Radius	180° Radius	270° Raw data	270° Radius
1	-	-	.572	2.012	2.517	.893	2.706
	-	-	.650	2.090	2.710	1.087	2.900
2	1.057	2.837	1.303	2.743	2.994	1.497	3.310
	1.234	3.014	1.521	2.961	3.114	1.710	3.523
3	1.668	3.448	1.906	3.346	3.455	2.031	3.844
	1.847	3.627	2.106	3.546	3.613	2.235	4.048
4	2.181	3.961	2.425	3.865	3.910	2.515	4.328
	2.338	4.118	2.596	4.036	4.045	2.676	4.489
5	2.660	4.44	2.896	4.336	4.195	2.951	4.764
	2.780	4.56	3.030	4.470	4.433	3.076	4.889
6	3.081	4.861	3.306	4.746	4.679	3.340	5.153
	3.173	4.953	3.438	4.878	4.784	3.452	5.265
7	3.465	5.245					
	3.558	5.338					

differential probe trace pattern shown in Figure 7. The differential probe gives the beam current at positions that are digitally displayed at the control consol. By knowing the beginning and end positions of the probe in the machine system one can measure the probe trace pattern, (measured as 8.29 inches) and taking the ratio of these numbers define a conversion factor that gives the position of all points on the probe trace pattern in units of the machine dimensions. The width of the peak was considered the radial length of the beam and the sharp edge of the peak is the outer radius of the beam. This procedure was verified visually by noting when the glow of the foil hole dissappeared when moving the differential probe from its outer most radius to inside the second turn. As was seen in Figures 4 and 9, some holes were flat on one edge and rounded on the other. Since the holes were not shaped the same, it was necessary to consider the width of the beam as the acceptable data.

Magnetic field data for input into the computer calculations was taken from the measured fields previously mentioned. A lagranian point-interpolation was done using the cyclotron settings to generate the raw field data, depending on the particle and its energy as well as the rf-frequency, main magnet and trim coils settings.[5]

FIGURE 9.--Hole patterns burned on stainless steel screens, exposed at 0°, 90°, and 270° simultaneously. On the 270° foil the screen was too short so the outside radius of the initial (0th) turn is slightly heated and burned, but not enough definition for data. (2nd run) 24 MeV deuterons.

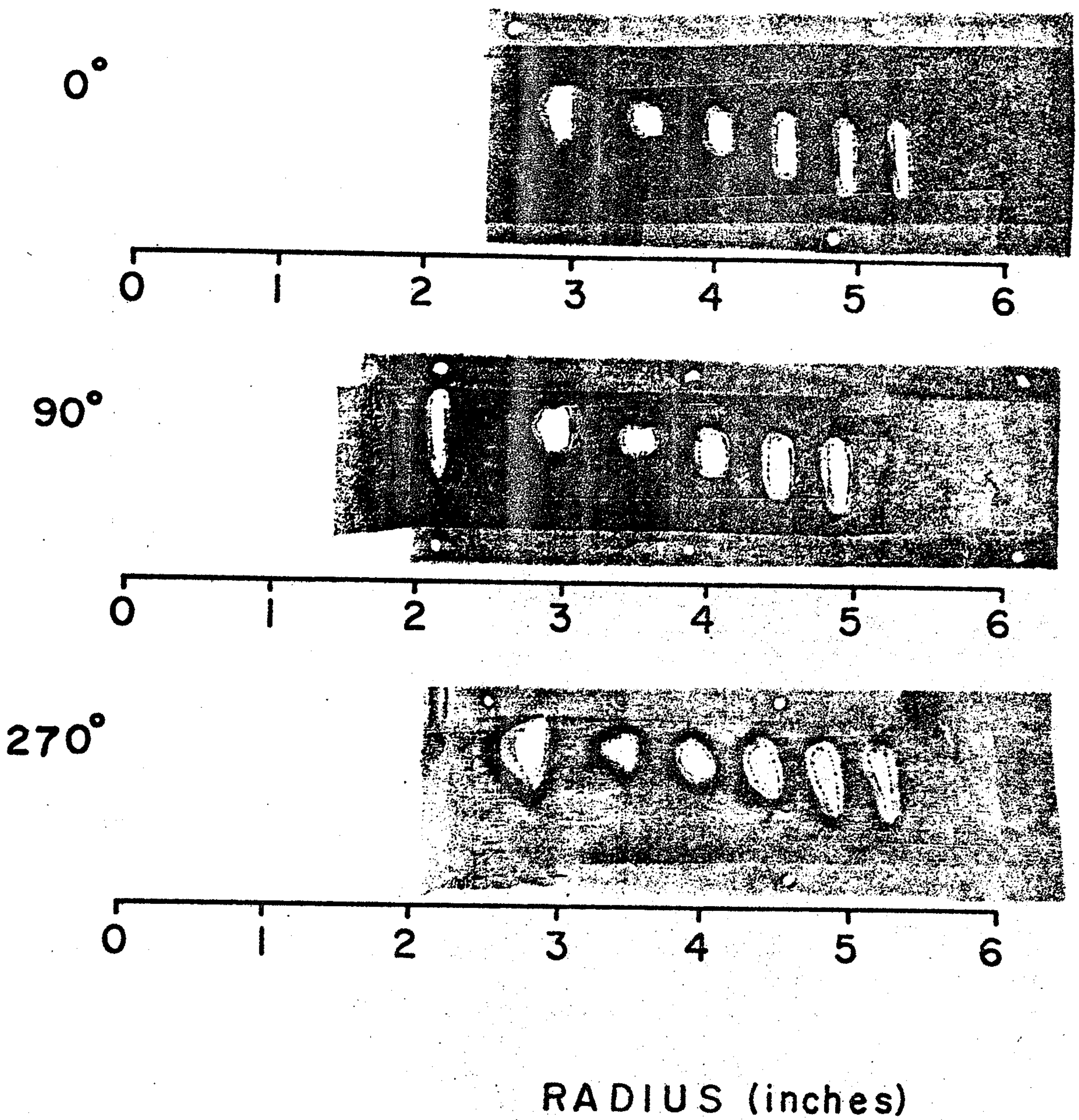

Figure 9

4. DATA ANALYSIS

4.1 CYCLONE Computer Orbit Code

Beam orbit calculations for this study were done using the precise orbit code known as CYCLONE. This code utilizes exact median plane radial equations of motion for particle trajectories in crossed electric and magnetic fields. Details of the electric fields are accounted for in three ways, which corresponds to the part of the program in which these various fields are used:

(a) Source-puller region; in which the first part of the program considers the initial turn and uses the source to puller electric field.

(b) "rf focusing" region; the second part of the program considers the first four turns and uses the large electric field;

(c) the main acceleration region utilizes a step-function time-dependent potential in much the same way as the idea of assuming step function energy gain at each acceleration gap.

CYCLONE also provides provisions for study of equilibrium orbits, electrostatic deflector and magnetic channel. However, none of these studies are included.

Out put from the CYCLONE program is provided in the appendices. Analysis of the CYCLONE program is presented here in the form of graphs, which compare the radius vs. turn numbers for various starting phases and radius vs turn number for the foil burned data presented earlier. In the use of this code it was necessary to pick the correct starting phase which would correspond to the foil burns. The method used initially was to run the program in succession changing the dee voltage until the beam is aligned with the radial slit on the initial turn at 1.713 inches radius for 180° as can be seen from Figure 10. However, the dee voltage can be closely approximated by using the differential probe trace to determine the number of turns and using the equation:

$$E_f/\eta = 4\, V_{dee} \sin[N\theta_{dee}/2]$$

where E_f is the final particle energy.

η = number of turns

N = Harmonic number

θ_{dee} = angular length of the dees.

Thus knowing the maximum energy gain per turn, it is possible to determine the approximate dee voltage.

FIGURE 10.--Plot of calculated orbit leaving the source at a starting time of -35° (rf-degrees), superimposed on a drawing of the N=2 central region geometry for 134° dees, in the MSU Cyclotron. Data experimentally gathered is indicated by the rectangles at all four positions, from foil burns and differential probe.

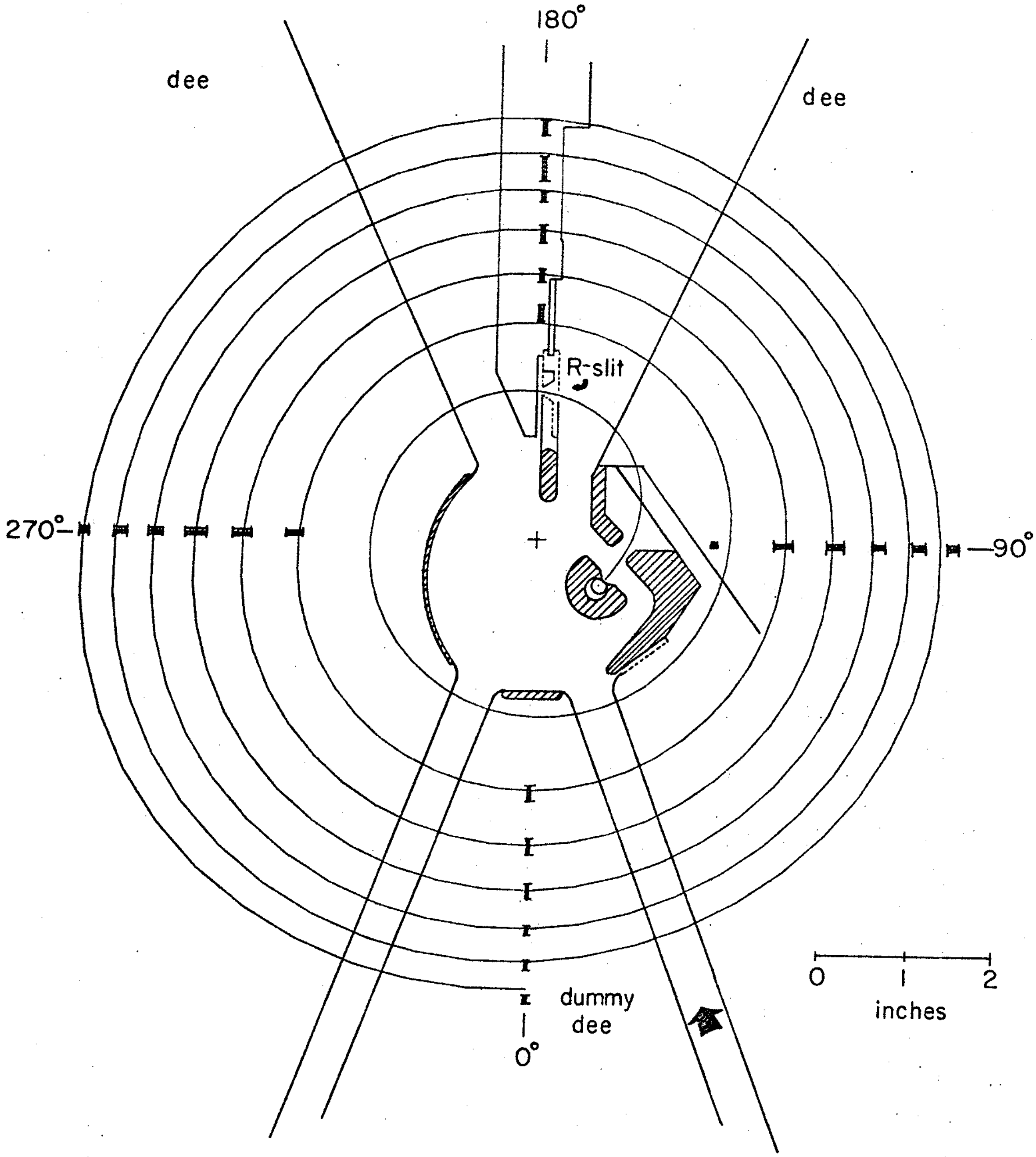

Figure 10

4.2 CYCLONE Calculations and Verification Analysis

In Figure 11, the results for one run are plotted against CYCLONE calculations for starting times (in rf-degrees) from -20° to -50° in 5° intervals. Figure 11a shows the results for the new fields and Figure 11b the results for the old fields. By comparing the width of the foil holes and the theoretical curve, one can compare which curves are accurate and therefore (since the only altered parameter are the electric fields), which fields correspond best to what actually exist in the Cyclotron machine. The width of the hole to some extent, is the degree of uncertainty in the beam position. Even though the measurements are accurate to within .001 inch, the center beam spot is still uncertain by the width of the burned hole. On the 0^{th} turn only the outer edge of the hole is well defined.

Examining first the old field data (Figure 11b), it is found that at -20° starting time, a close fit is possible for data at 270° and 0° out to the fifth turn. In the sixth and seventh turns only the 0° data is closely fitted by the curve. This phenomenon is observed for the other starting times as well to such an extent that none can give a close correlation for all the holes at once. It becomes necessary to change starting times to fit the data only at a specific angle.

FIGURE 11.--Plot of inside and outside radii of foil data for the first data run, against turn number. Plot (a) gives theoretical curve from the CYCLONE code of radius-vs-turn number for various starting times using the new electric fields. The curves for the old fields are shown for comparison in (b). No data shown for 180°.

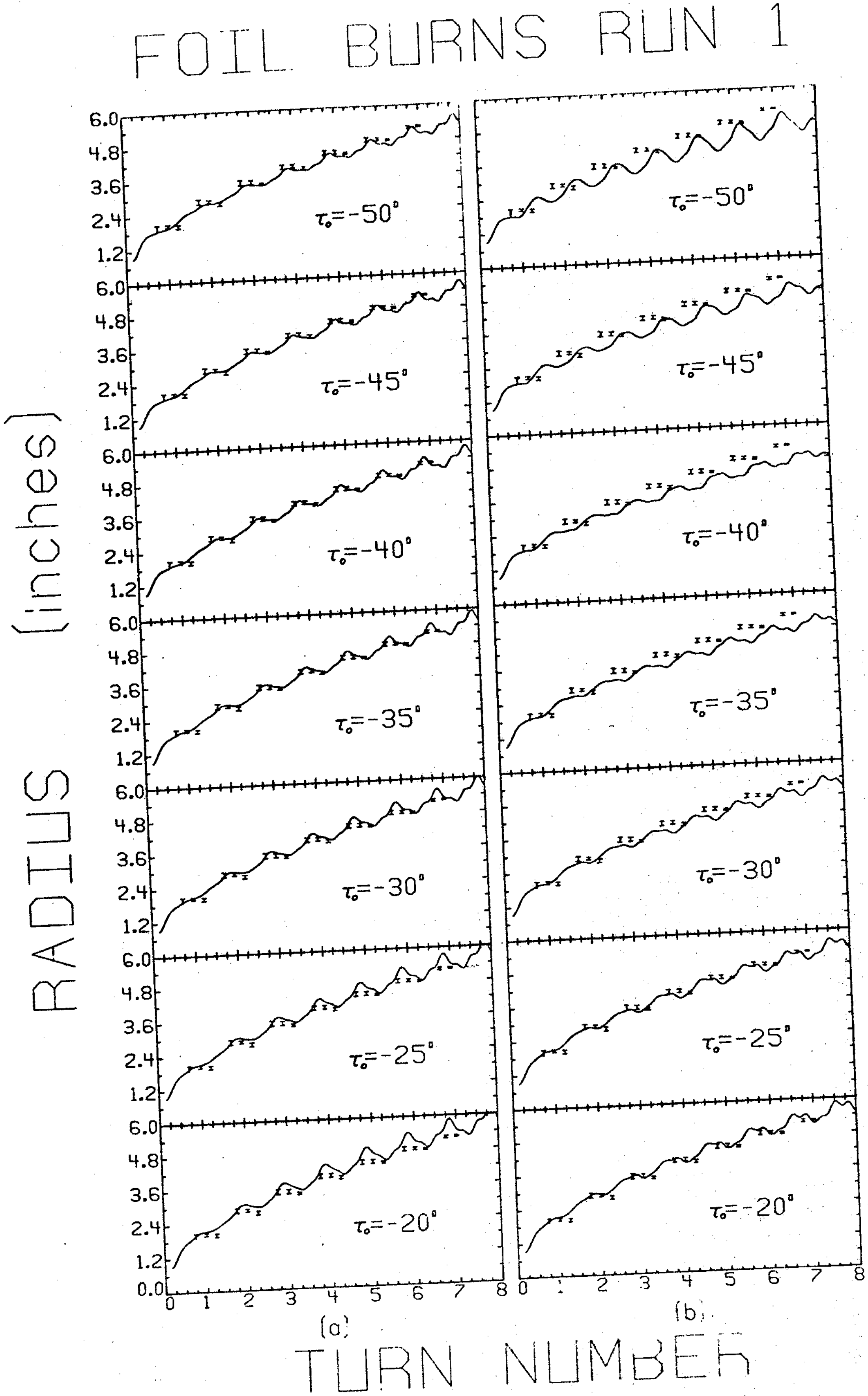
FOIL BURNS RUN 1
RADIUS (inches)
TURN NUMBER
τo=-50°
τo=-45°
τo=-40°
τo=-35°
τo=-30°
τo=-25°
τo=-20°
(a)
(b)
6.0
4.8
3.6
2.4
1.2
0.0
0 1 2 3 4 5 6 7 8

Figure 11

With the new fields (Figure 11a) the observation tends to be similar with the exception that for one starting time it is possible to fit accurately all the turns at all the data angles simultaneously, namely -35° and -40°. By plotting the different starting times for this run it is possible to observe the position of the Cyclone data shifting radially at the turns but still restricted to pass through the initial radial slit at 180°. The accuracy of the source to puller field and large electric field for the old data account for the shift in position according to turn number. In contrast Figure 12a fully illustrates the close correlation of Cyclone theoretical calculations to the measured field data. Data in Figure 12 also includes the 180° beam position making the analysis complete for four different sectors of the machine. Accurate agreement between experimental and theoretical positions was determined to be approximately .01 to .2 inches. Using the data from the second run this is illustrated better by introducing a parameter corresponding to the change in the position of the beam by Cyclone and the foil burns. Therefore we denote:

$$\Delta R = R_{\text{foil burns}} - R_{\text{cyclone}}$$

as this change in position. Data for the foil burns, however, is presented as an inside and outside radius. Therefore, the centroid of this hole was considered the

FIGURE 12.--Plot of inside and outside radii of foil data for the second data run, against turn number. Theoretical curves for various starting times are plotted for the new fields (a) and the old fields (b).

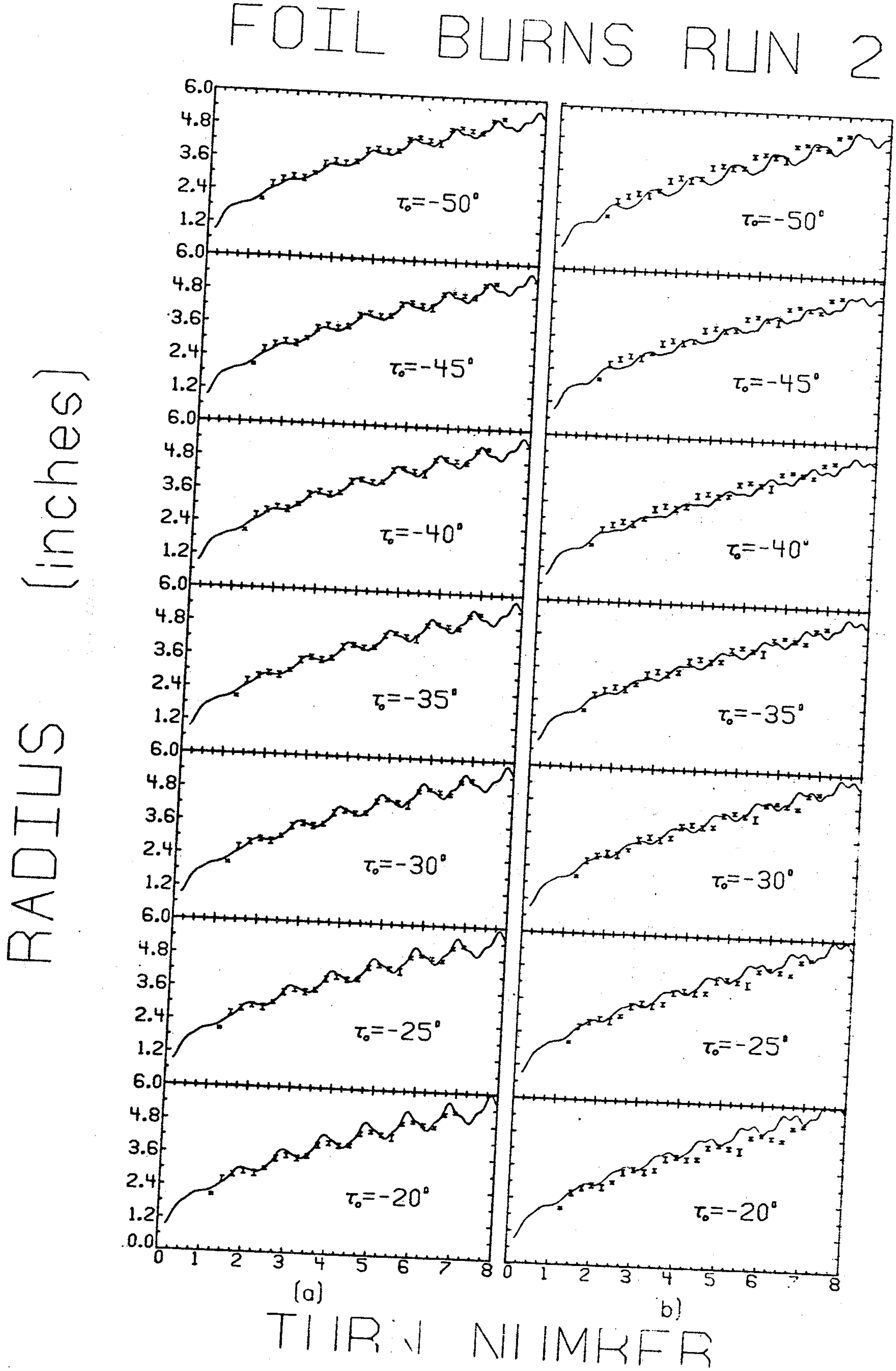
FOIL BURNS RUN 2
RADIUS (inches)
TURN NUMBER
6.0
4.8
3.6
2.4
1.2
0.0
0 1 2 3 4 5 6 7 8
(a)
b)
τ₀=-50°
τ₀=-45°
τ₀=-40°
τ₀=-35°
τ₀=-30°
τ₀=-25°
τ₀=-20°

Figure 12

beam position and this was considered R_f for the ΔR calculations. These calculations are presented in Table V thru Table VIII. In Figure 13 ΔR is plotted against starting time for successive turns, at each angular position of the data. By choosing a starting time at those turns where the line crosses 0.00 inches, it is easy to pick the initial starting time which gives close correlation to the foil data for this particular N=2 run. In this way a close determination of the initial phase at which the peak intensity portion of the beam leaves the ion source and consequently its phase dependence in the initial few turns can be studied. This is also a means of determining if the foil holes can be fitted at only one angular position at a time easily. In Figure 13 at 0° this seems true since the slope of the lines indicates a wide spread in starting time yielding a large range in data matching. The other angles indicate that -35° starting time should give accurate results for the second, third and fourth turns with a slightly larger spread at the fifth and sixth turns.

FIGURE 13.--ΔR-vs-starting time for the four burn positions, showing comparison of foil position to cyclone calculated radius. Each turn of the data is indicated. Note the greatly expanded radial scale contrasted to figures 11 and 12.

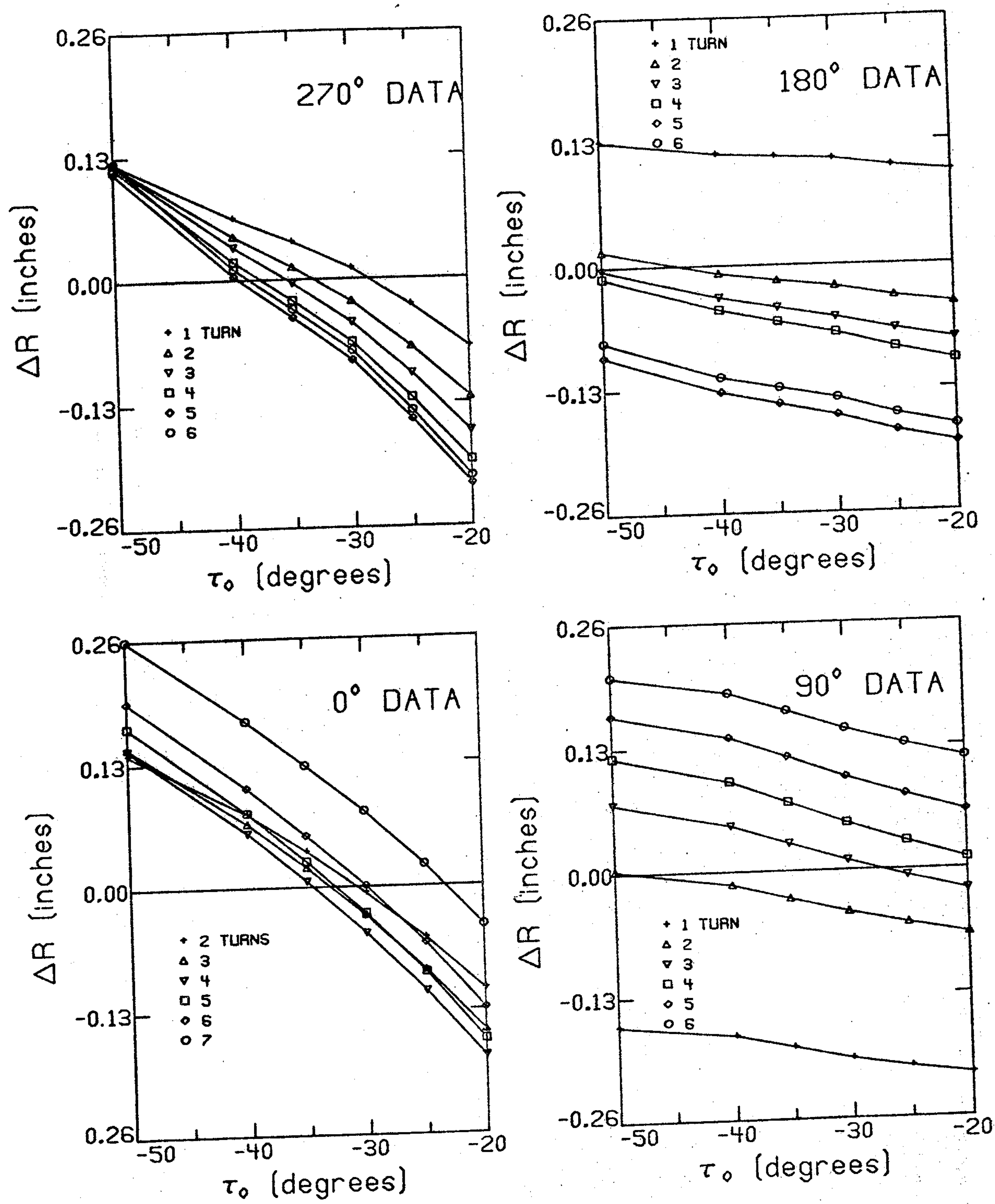
270° DATA
0.26
0.13
0.00
-0.13
-0.26
ΔR (inches)
+ 1 TURN
△ 2
▽ 3
□ 4
◇ 5
○ 6
-50
-40
-30
-20
τ₀ (degrees)
180° DATA
0.26
0.13
0.00
-0.13
-0.26
ΔR (inches)
+ 1 TURN
△ 2
▽ 3
□ 4
◇ 5
○ 6
-50
-40
-30
-20
τ₀ (degrees)
0° DATA
0.26
0.13
0.00
-0.13
0.26
ΔR (inches)
+ 2 TURNS
△ 3
▽ 4
□ 5
◇ 6
○ 7
-50
-40
-30
-20
τ₀ (degrees)
90° DATA
0.26
0.13
0.00
-0.13
-0.26
ΔR (inches)
+ 1 TURN
△ 2
▽ 3
□ 4
◇ 5
○ 6
-50
-40
-30
-20
τ₀ (degrees)

Figure 13

TABLE V.--ΔR-vs-turn number data at various starting times for the 0° data. Radii are presented in inches accurate to .001 inch.

τ_o=-20°		τ_o=-25°		τ_o=-30°	
Turn #	ΔR	Turn #	ΔR	Turn #	ΔR
2	-.10917	2	-.05425	2	-.00680
3	-.15193	3	-.08832	3	-.03048
4	-.17938	4	-.11047	4	-.04890
5	-.16167	5	-.09047	5	-.02808
6	-.12886	6	-.05992	6	.00073
7	-.04187	7	.02213	7	.07880

τ_o=-35°		τ_o=-40°		τ_o=-50°	
2	.03717	2	.07729	2	.14044
3	.02008	3	.06690	3	.14726
4	.00598	4	.05696	4	.14535
5	.02654	5	.07793	5	.16879
6	.05357	6	.10421	6	.19491
7	.12753	7	.17430	7	.25954

TABLE VI.--ΔR-vs-turn number data at various starting times for 90° data. ΔR are in inches ±.001 inch.

τ_o=-20°		τ_o=-25°		τ_o=-30°	
Turn #	ΔR	Turn #	ΔR	Turn #	ΔR
1	-.21456	1	-.20647	1	-.19713
2	-.06761	2	-.05594	2	-.04354
3	-.02155	3	-.00672	3	.01021
4	.01094	4	.02952	4	.04973
5	.06107	5	.07913	5	.09795
6	.11762	6	.13233	6	.14858

τ_o=-35°		τ_o=-40°		τ_o=-50°	
1	-.18418	1	-.17095	1	-.15976
2	-.02854	2	-.01317	2	.00300
3	.02899	3	.04830	3	.07280
4	.07222	4	.09483	4	.12131
5	.11978	5	.14101	5	.16504
6	.16822	6	.8740	6	.20568

TABLE VII.--ΔR-vs-turn number data at various starting times for the 180° data. Radii are presented in inches accurate to .001 inch.

τ_o=-20°		τ_o=-25°		τ_o=-30°	
Turn #	ΔR	Turn #	ΔR	Turn #	ΔR
1	.09764	1	.10317	1	.11120
2	-.04084	2	-.03301	2	-.02233
3	-.07833	3	-.06744	3	-.05468
4	-.10045	4	-.08683	4	-.07072
5	-.18726	5	-.17445	5	-.15749
6	-.16931	6	-.15635	6	-.13934

τ_o=-35°		τ_o=-40°		τ_o=-50°	
1	.11449	1	.11699	1	.13138
2	-.01574	2	-.00821	2	.01655
3	-.04401	3	-.03303	3	-.00321
4	-.05878	4	-.04592	4	-.01125
5	-.14496	5	-.13258	5	-.09423
6	-.12820	6	-.11696	6	-.07866

TABLE VIII.--ΔR-vs-turn number data at various starting times for the 180° data. Radii are in inches ±.001 inch.

τ_o=-20°		τ_o=-25°		τ_o=-30°	
Turn #	ΔR	Turn #	ΔR	Turn #	ΔR
1	-.07183	1	-.02733	1	.01148
2	-.12476	2	-.07124	2	-.02321
3	-.16068	3	-.09939	3	-.04513
4	-.19118	4	-.12493	4	-.06577
5	-.21657	5	-.14746	5	-.08504
6	-.20827	6	-.13803	6	-.07487

τ_o=-35°		τ_o=-40°		τ_o=-50°	
1	.04004	1	.06503	1	.12410
2	.01288	2	.04565	2	.12294
3	-.00354	3	.03447	3	.12303
4	-.02175	4	.01894	4	.11937
5	-.03968	5	.00385	5	.11381
6	-.03093	6	.01143	6	.12394

5. CONCLUSIONS

It has been shown that this experimental procedure is useful in the prediction of a good starting time and thereby a good starting phase. The orbit radii and their correlation to theoretical predictions seem to give a clue that a starting time of -35° to -40° gives a precise initial phase that best fits all the data. It is therefore concluded that this range for the starting time can be translated back to the actual machine thru the starting phase of the particles and thereby give better operation in the second harmonic mode.

This study of the central region electric fields has made it possible to substantiate our theoretical predictions. This investigation confirms that the new electric fields are accurate and reliable for future central region studies.

REFERENCES

1. Adventures in Experimental Physics, Issue 2(1972), p. i.
2. W. P. Johnson, Radio-Frequency System of the MSU Cyclotron, Proceedings of the International Conference on Sector-Focused Cyclotrons and Meson Factories, CERN, April 1963.
3. B. T. Smith, Michigan State University Cyclotron Project Internal Report, MSUCP-8, November, 1960.
4. R. Berg, Michigan State University Cyclotron Project Internal Report, MSUCP-14, January 1963.
5. R. Berg, H. G. Blosser and W. P. Johnson, Michigan State University Cyclotron Project Internal Report, MSUCP-22, August 1966.
6. M. Reiser, Michigan State University Cyclotron Project Internal Report, MSUCP-20, June 1964.
7. H. G. Blosser, "Problems and Performances in the Cyclotron Central Region," IEEE Trans. Nucl. Sci. NS-13 (14), 1966, (1-14).
8. Larry L. Learn, Private communication.
9. M. Reiser and J. Kopf, Automatic Electrolytic Tank and Digital Computer Program for Calculations of Ion Trajectories in Crossed Electric and Magnetic Fields, The Review of Scientific Instruments Vol. 36, No. 7, July 1965.

10. D. A. Johnson, Private communication.

11. H. G. Blosser, "Physics 961--Winter Term, 1971" Internal Report, MSU Cyclotron Laboratory (1972), p. 76.

APPENDIX

TABLE IX.--Cyclone calculations output for 24 MeV deuterons utilizing the new electric fields in the second run. Starting time is $-35°$ (rf-degrees).

CYCLONE-III

SMALL E FIELD 1.06.9-S LARGE E FIELD 2.138.2A B FIELD 24.00 0 FIRST HARMONIC
E3 = 1875.581 J = 1 A = 176.94981 B = 13.91975
RF FREQ = 20.75000 DEE VOLTAGE = 47.49001 HARMONIC NR = 2
DEE WIDTH = 138.00 FIRST GAP AT 21.00
LARGE FIELD ROTATED BY 45.00 DEGREES
GAPS AT 21.00 159.00 201.00 339.00 DEGREES
TRANSIT TIME EFFECTS INCLUDED IN PART 3
ALPHA1 = 20.00 ALPHA2 = 125.00 ALPHA3 = 135.00 ALPHA4 = .50
R1 = .8750 R2 = .5160 R3 = .1100 W/P = .0200

RAY NUMBER 0 PART ONE STEP = 1.874999

REV	THETA	R	PR	PHI	E	TAU	XI	ETA	V
0	60.7166	.916902	.004955	-66.4331	.000010	-35.0000	.000000	.000000	.000030
0	60.7387	.916999	.006655	-64.6024	.000020	-33.1250	-.000003	.000368	-.000219
0	60.7686	.917124	.008339	-62.7872	.000034	-31.2500	-.000012	.000863	-.000562
0	60.8067	.917279	.010018	-60.9884	.000052	-29.3750	-.000030	.001491	-.001007
0	60.8533	.917450	.011710	-59.2065	.000075	-27.5000	-.000058	.002258	-.001568
0	60.9088	.917470	.013438	-57.4425	.000105	-25.6250	-.000099	.003171	-.002260
0	60.9738	.917910	.015227	-55.6976	.000141	-23.7500	-.000154	.004238	-.003101
0	61.0438	.918181	.017103	-53.9727	.000185	-21.8750	-.000226	.005468	-.004115
0	61.1344	.918483	.019099	-52.2689	.000239	-20.0000	-.000316	.006871	-.005330
0	61.2314	.918821	.021250	-50.5879	.000304	-18.1250	-.000425	.008458	-.006779
0	61.3405	.919196	.023593	-48.9310	.000363	-16.2500	-.000555	.010242	-.008503
0	61.4624	.919612	.026170	-47.2938	.000476	-14.3750	-.000708	.012237	-.010548
0	61.5981	.920074	.029023	-45.6962	.000588	-12.5000	-.000886	.014457	-.012973
0	61.7437	.920586	.032198	-44.1223	.000722	-10.6250	-.001089	.016920	-.015847
0	61.9151	.921154	.035737	-42.5801	.000851	-8.7500	-.001320	.019644	-.019253
0	62.0936	.921785	.039740	-41.0722	.001074	-6.8750	-.001579	.022652	-.023340
0	62.3009	.922483	.044291	-39.6019	.001308	-5.0000	-.001871	.025971	-.028300
0	62.5230	.923271	.049345	-38.1728	.001559	-3.1250	-.002199	.029632	-.034239
0	62.7690	.924142	.054819	-36.7890	.001921	-1.2500	-.002566	.033662	-.041233
0	63.0376	.925103	.060601	-35.4502	.002305	.6250	-.002980	.038083	-.049312
0	63.3307	.926173	.066552	-34.1513	.002737	2.5000	-.003446	.042913	-.058425
0	63.6495	.927337	.072536	-32.9221	.003215	4.3750	-.003972	.048159	-.068494
0	63.9919	.928605	.078948	-31.7337	.003750	6.2500	-.004566	.053831	-.079812
0	64.3615	.929983	.085742	-30.5980	.004352	8.1250	-.005234	.059946	-.092582
0	64.7684	.931479	.093072	-29.5169	.005028	10.0000	-.005982	.066523	-.107006
0	65.1837	.933107	.101056	-28.4924	.005790	11.8750	-.006820	.073581	-.123350
0	65.6337	.934868	.109637	-27.5274	.006653	13.7500	-.007753	.081148	-.141980
0	66.1245	.936785	.119301	-26.6240	.007602	15.6250	-.008790	.089245	-.162798
0	66.6416	.938865	.129355	-25.7833	.008645	17.5000	-.009935	.097885	-.185561
0	67.1991	.941127	.140362	-25.0053	.009768	19.3750	-.011204	.107076	-.210503
0	67.7731	.943572	.152456	-24.2901	.010971	21.2500	-.012587	.116825	-.237518
0	68.4810	.946231	.165273	-23.6369	.012251	23.1250	-.014090	.127136	-.266521
0	69.0228	.949106	.178250	-23.0455	.013619	25.0000	-.015724	.138013	-.298159
0	69.6952	.952199	.191062	-22.5154	.015025	26.8750	-.017509	.149451	-.331119
0	70.3962	.955506	.204315	-22.0425	.016436	28.7500	-.019453	.161425	-.364686
0	71.1249	.959049	.219184	-21.6248	.017949	30.6250	-.021553	.173928	-.401373
0	71.8819	.962855	.235637	-21.2639	.019626	32.5000	-.023813	.186990	-.442321
0	72.6670	.966937	.251941	-20.9530	.021277	34.3750	-.026243	.200512	-.484480
0	73.4767	.971291	.268288	-20.7033	.022846	36.2500	-.028846	.214744	-.524978
0	74.3081	.975927	.285691	-20.4911	.024407	38.1250	-.031613	.229353	-.566227
0	75.1594	.980851	.303683	-20.3198	.025955	40.0000	-.034539	.244423	-.608233
0	76.0288	.986097	.321779	-20.1826	.027500	41.8750	-.037628	.259934	-.651300
0	76.9147	.991632	.339333	-20.0794	.028990	43.7500	-.040889	.275864	-.694057

0	77.8143	.997461	.356971	-20.0036	.030362	45.6250	-.044325	.292173	-.734694
0	78.7245	1.003584	.374530	-19.9489	.031617	47.5000	-.047924	.308821	-.773132
0	79.6424	1.009997	.391504	-19.9038	.032760	49.3750	-.051681	.325768	-.809395
0	80.5659	1.016638	.407491	-19.8818	.033789	51.2500	-.055600	.342978	-.843302
0	81.4924	1.023629	.421345	-19.8598	.034628	53.1250	-.059689	.360401	-.872120
0	82.4193	1.030783	.432708	-19.8386	.035283	55.0000	-.063963	.377980	-.895584
0	83.3444	1.038104	.441563	-19.8138	.035774	56.8750	-.068441	.395658	-.914039
0	84.2665	1.045555	.448386	-19.7831	.036161	58.7500	-.073142	.413395	-.929307
0	85.1849	1.053107	.453461	-19.7448	.036465	60.6250	-.078083	.431156	-.941989
0	86.0990	1.060731	.456957	-19.6979	.036701	62.5000	-.083281	.448916	-.952431
0	87.0033	1.068400	.459122	-19.6417	.036875	64.3750	-.088749	.466648	-.960630
0	87.9128	1.076088	.460407	-19.5757	.037016	66.2500	-.094497	.484332	-.967695
0	88.8123	1.083814	.460950	-19.4996	.037119	68.1250	-.100530	.501954	-.973285
0	89.7065	1.091530	.460845	-19.4131	.037192	70.0000	-.106851	.519498	-.977500
0	90.5956	1.099241	.460393	-19.3161	.037250	71.8750	-.113462	.536951	-.981297
0	91.4793	1.106944	.459675	-19.2037	.037290	73.7500	-.120362	.554306	-.984155
0	92.3578	1.114633	.458662	-19.0905	.037322	75.6250	-.127549	.571554	-.986744
0	93.2310	1.122301	.457394	-18.9621	.037343	77.5000	-.135025	.588685	-.988580
0	94.0901	1.129947	.455985	-18.8231	.037356	79.3750	-.142785	.605694	-.990003
0	94.9620	1.137569	.454438	-18.6739	.037366	81.2500	-.150829	.622575	-.991235
0	95.8199	1.145163	.452758	-18.5148	.037372	83.1250	-.159153	.639321	-.992155
0	96.6728	1.152727	.450986	-18.3456	.037376	85.0000	-.167756	.655927	-.992906
0	97.5209	1.160263	.449119	-18.1667	.037378	86.8750	-.176634	.672388	-.993665
0	98.3642	1.167766	.447157	-17.9783	.037379	88.7500	-.185785	.688700	-.994125
0	99.2028	1.175235	.445105	-17.7806	.037379	90.6250	-.195206	.704857	-.994357
0	100.0369	1.182669	.442971	-17.5738	.037379	92.5000	-.204895	.720855	-.994689
0	100.8665	1.190067	.440758	-17.3581	.037377	94.3750	-.214848	.736689	-.995190
0	101.6917	1.197427	.438464	-17.1335	.037376	96.2500	-.225063	.752356	-.995447
0	102.5127	1.204747	.436089	-16.9004	.037374	98.1250	-.235537	.767850	-.995755
0	103.3295	1.212029	.433676	-16.6591	.037373	100.0000	-.246267	.783168	-.995969
0	104.1423	1.219259	.431134	-16.4096	.037372	101.8750	-.257250	.798305	-.996100
0	104.9510	1.226465	.428649	-16.1521	.037380	103.7500	-.268483	.813258	-.996283
0	105.7561	1.233619	.425960	-15.8871	.037382	105.6250	-.279963	.828024	-.996140
0	106.5572	1.240726	.423021	-15.6144	.037371	107.5000	-.291688	.842595	-.995944
0	107.3547	1.247724	.420118	-15.3344	.037365	109.3750	-.303654	.856966	-.996337
0	108.1485	1.254793	.417210	-15.0470	.037362	111.2500	-.315857	.871134	-.996555

PART TWO STEP = 7.499997

REV	THETA	R	PR	PHI	E	TAU	XE9	PXE9
0	108.1485	1.254793	.417210	-15.0470	.037362	111.2500		
0	112.4999	1.292883	.401706	-13.3336	.037521	121.6662		
0	119.9999	1.355475	.374186	-9.9103	.038195	140.0896		
0	127.4999	1.417405	.350987	-6.1163	.040051	158.8836		
0	134.9999	1.474857	.335645	-2.3641	.044045	177.5356		
0	142.4999	1.527420	.314591	.8579	.050088	-164.1423		
0	149.9999	1.575005	.286781	3.3564	.056637	-146.6439		
0	157.4999	1.616650	.257035	5.2754	.062155	-129.7251		
0	164.9999	1.652137	.230709	6.8774	.061838	-113.1228		
0	172.4999	1.684434	.205624	8.4331	.067469	-96.5471		
0	179.9999	1.713197	.179229	10.1543	.067530	-79.8459		
0	187.4999	1.738194	.152814	12.0293	.069401	-62.9709		
0	194.9999	1.759457	.133806	13.7230	.073667	-46.2712		
0	202.4999	1.777577	.115871	15.0178	.079155	-29.9824		
0	209.9999	1.793413	.110950	15.7920	.086357	-14.2053		
0	217.4999	1.808677	.113515	16.1006	.092422	1.1003		
0	224.9999	1.824285	.119966	16.0981	.096985	16.0979		
0	232.4999	1.840644	.126834	15.9392	.099917	30.9330		

0	239.9999	1.857778	.131704	15.7532	.101482	45.7529
0	247.4999	1.875471	.134369	15.6316	.102150	60.6316
0	254.9999	1.893457	.134434	15.6134	.102431	75.6182
0	262.5000	1.911476	.131519	15.7361	.102490	90.7361
0	270.0000	1.929039	.125773	15.9927	.102456	105.9927
0	277.5000	1.945760	.117059	16.3838	.102434	121.3838
0	285.0000	1.961207	.105524	16.8089	.102436	136.8989
0	292.5000	1.974798	.092114	17.5203	.102560	152.5203
0	300.0000	1.986893	.077383	18.2224	.102835	168.2224
0	307.5000	1.996753	.063264	18.9739	.103404	-176.0261
0	315.0000	2.004839	.052564	19.7275	.104591	-160.2725
0	322.5000	2.011862	.049338	20.4155	.106782	-144.5245
0	330.0000	2.019320	.058216	20.9352	.110662	-129.0618
0	337.5000	2.026884	.050945	21.1995	.115520	-113.8005
0	345.0000	2.033302	.045198	21.2593	.118180	-98.7407
0	352.5000	2.039201	.044331	21.2720	.118440	-83.7280
1	.0000	2.045494	.053679	21.3519	.117917	-68.6481
1	30.0000	2.095099	.113122	20.4045	.143059	-9.5555
1	60.0000	2.154235	.137898	16.2433	.152104	46.2433
1	90.0000	2.235182	.173939	13.4355	.152198	103.4355
1	120.0000	2.331056	.182010	12.0132	.153941	162.9132
1	150.0000	2.422527	.152095	13.4839	.168787	-136.5165
1	180.0000	2.499011	.133188	13.2483	.177417	-76.7520
1	210.0000	2.565326	.125200	13.3262	.195371	-16.6741
1	240.0000	2.648066	.195160	11.9202	.205540	41.9199
1	270.0000	2.762059	.214011	12.1404	.209251	102.1404
1	300.0000	2.863557	.129655	14.7738	.209662	154.7788
1	330.0000	2.899584	.002745	18.3943	.217962	-131.6057
2	.0000	2.888329	-.029558	20.5541	.224768	-60.4459
2	30.0000	2.871330	-.022268	21.3135	.244498	-8.6805
2	60.0000	2.869520	.010150	19.2971	.255275	49.2970
2	90.0000	2.850539	.037630	17.0102	.255463	107.0102
2	120.0000	2.916049	.104265	15.1339	.256603	165.1338
2	150.0000	2.984394	.149895	13.7275	.270195	-136.2728
2	180.0000	3.069742	.164513	12.1147	.279862	-77.8855
2	210.0000	3.149466	.153808	11.2146	.293754	-18.7856
2	240.0000	3.253497	.246757	9.3754	.310739	39.8782
2	270.0000	3.403621	.283704	10.6318	.311147	100.6318
2	300.0000	3.534050	.149191	14.0208	.311402	164.0208
2	330.0000	3.560017	-.046209	18.5007	.318659	-131.4993
3	.0000	3.517423	-.082541	21.5539	.324361	-65.4461
3	30.0000	3.475807	-.061985	22.2547	.342091	-7.0453
3	60.0000	3.448577	-.054827	21.8217	.358919	51.8216
3	90.0000	3.417009	-.001666	19.0775	.358051	109.9775
3	120.0000	3.415525	.060060	17.7493	.359759	167.7493
3	150.0000	3.479084	.172133	15.7175	.372096	-134.2827
3	180.0000	3.576011	.156795	13.3809	.382253	-76.1104
3	210.0000	3.692706	.165907	12.8767	.403639	-17.1235
3	240.0000	3.773003	.275567	11.7036	.414536	41.7034
3	270.0000	3.949832	.340728	12.7319	.414788	102.7319
3	300.0000	4.102077	.154204	16.4844	.414984	166.4844
3	330.0000	4.109358	-.106644	21.2595	.421184	-128.7405
4	.0000	4.033522	-.127156	24.5254	.425426	-65.4746
4	30.0000	3.977072	-.072232	25.9913	.454453	-4.0087
4	60.0000	3.940479	-.093720	25.1930	.463317	55.1930
4	90.0000	3.878778	-.118563	23.5340	.463395	113.5340
4	120.0000	3.852175	.040033	21.0686	.463872	171.0686
4	150.0000	3.921074	.206055	18.7124	.474897	-131.2880
4	180.0000	4.036781	.204988	16.9292	.484792	-73.0710

4	210.0000	4.121333	.145284	16.0063		
4	240.0000	4.231733	.203705	14.9505	.508859	-13.9939
4	270.0000	4.430248	.393410	16.1609	.515827	‾44.9802
4	300.0000	4.602203	.151032	20.1289	.518369	106.1609
4	330.0000	4.584793	-.176030	25.0020	.519084	170.1289
5	.0000	4.473464	-.169561	28.2178	.524381	-124.9980
5	30.0000	4.409126	-.069246	29.5156	.530241	-61.7822
5	60.0000	4.359019	-.119009	28.3048	.559140	-.4844
5	90.0000	4.283522	-.173681	27.1851	.567183	‾58.8048
5	120.0000	4.238065	.032569	24.5009	.567210	117.1861
5	150.0000	4.319471	.255507	21.9248	.567540	174.5009
5	180.0000	4.458061	.228495	20.3135	.577294	-128.0757
5	210.0000	4.542496	.126851	19.6338	.585413	-69.6868
5	240.0000	4.648775	.304693	18.8340	.612369	-10.3665
5	270.0000	4.866681	.440659	20.2048	.622034	‾48.8337
					.622111	110.2048

PART THREE

REV	THETA	R	PR	PHI	$\dot{\Xi}$	TAU	$\bar{X}E\theta$	$P\dot{X}E\theta$
5	270.0000	4.866681	.440659	20.2046	.622111	¯110.2046		
6	.0000	4.853429	-.216741	32.6224	.630403	-57.3776		
6	180.0000	4.860200	.248558	24.4451	.683130	-65.5552		
7	.0000	5.163975	-.245388	36.5050	.727088	-53.4950		

TABLE X.--Cyclone calculations output for 24 MeV deuterons utilizing the new electric fields in the second run. Starting time is -40° (rf-degrees).

CYCLONE-III

SMALL E FIELD 1.05.9-S LARGE E FIELD 2.138.2A B FIELD 24.00 0 FIRST HARMONIC
E9 = 1675.531 J = 1 A = 176.94931 B = 13.91975
RF FREQ = 20.75000 DEE VOLTAGE = 45.95100 HARMONIC NO = 2
DEE WIDTH = 138.00 FIRST GAP AT 21.00
LARGE FIELD ROTATED BY 45.00 DEGREES
GAPS AT 21.00 159.00 201.00 339.00 DEGREES
TRANSIT TIME EFFECTS INCLUDED IN PART 3
ALPHA1 = 20.00 ALPHA2 = 125.00 ALPHA3 = 135.00 ALPHA4 = .00
R1 = .8750 R2 = .5160 R3 = .1100 W/P = .0200

RAY NUMBER 0 PART ONE STEP = 1.874999

REV	THETA	R	PR	PHI	E	TAU	XI	ETA	V
0	60.7166	.916902	.004955	-71.4331	.000010	-40.0000	.000000	.000000	.000030
0	60.7383	.916997	.006469	-69.5017	.000019	-38.1250	-.000003	.000352	-.000215
0	60.7673	.917118	.007976	-67.7645	.000031	-36.2500	-.000012	.000840	-.000545
0	60.8035	.917264	.009494	-65.9821	.000047	-34.3750	-.000029	.001439	-.000959
0	60.8476	.917436	.011007	-64.1952	.000067	-32.5000	-.000057	.002164	-.001498
0	60.8999	.917633	.012566	-62.4248	.000092	-30.6250	-.000096	.003024	-.002146
0	60.9609	.917857	.014181	-60.6718	.000124	-28.7500	-.000149	.004025	-.002930
0	61.0311	.918108	.015875	-58.9372	.000162	-26.8750	-.000217	.005176	-.003870
0	61.1111	.918389	.017677	-57.2222	.000208	-25.0000	-.000302	.006485	-.004990
0	61.2015	.918701	.019617	-55.5281	.000264	-23.1250	-.000406	.007965	-.006320
0	61.3031	.919047	.021727	-53.8562	.000331	-21.2500	-.000530	.009625	-.007895
0	61.4166	.919430	.024046	-52.2081	.000411	-19.3750	-.000675	.011479	-.009756
0	61.5427	.919853	.026612	-50.5854	.000507	-17.5000	-.000843	.013541	-.011952
0	61.6825	.920322	.029467	-48.9900	.000621	-15.6250	-.001036	.015827	-.014545
0	61.8370	.920842	.032655	-47.4239	.000757	-13.7500	-.001254	.018352	-.017604
0	62.0071	.921418	.036209	-45.8892	.000919	-11.8750	-.001499	.021137	-.021226
0	62.1944	.922057	.040279	-44.3858	.001117	-10.0000	-.001774	.024206	-.025502
0	62.4007	.922769	.044854	-42.9263	.001356	-8.1250	-.002081	.027587	-.030850
0	62.6274	.923562	.049877	-41.5047	.001640	-6.2500	-.002425	.031309	-.037090
0	62.8759	.924441	.055262	-40.1269	.001972	-4.3750	-.002810	.035395	-.044350
0	63.1477	.925414	.060895	-38.7953	.002352	-2.5000	-.003241	.039867	-.052644
0	63.4432	.926481	.066645	-37.5114	.002777	-.6250	-.003727	.044737	-.061889
0	63.7630	.927646	.072547	-36.2750	.003247	1.2500	-.004274	.050013	-.072127
0	64.1075	.928912	.078814	-35.0906	.003776	3.1250	-.004869	.055708	-.053553
0	64.4785	.930287	.085538	-33.9569	.004372	5.0000	-.005578	.061839	-.096641
0	64.8751	.931780	.092817	-32.8772	.004942	6.8750	-.006348	.068424	-.111298
0	65.3017	.933399	.100792	-31.8534	.005799	8.7500	-.007207	.075488	-.127935
0	65.7559	.935159	.109524	-30.8838	.006653	10.6250	-.008162	.083055	-.146795
0	66.2424	.937070	.118904	-29.9849	.007596	12.5000	-.009220	.091146	-.167746
0	66.7583	.939143	.128847	-29.1426	.008617	14.3750	-.010390	.099772	-.190589
0	67.3062	.941392	.139921	-28.3623	.009725	16.2500	-.011675	.108942	-.215598
0	67.8844	.943835	.151947	-27.6438	.010910	18.1250	-.013076	.118664	-.242597
0	68.4934	.946485	.164707	-26.9868	.012177	20.0000	-.014595	.128941	-.271763
0	69.1331	.949350	.177513	-26.3912	.013529	21.8750	-.016247	.139780	-.303276
0	69.8022	.952428	.190204	-25.8559	.014912	23.7500	-.018030	.151174	-.335922
0	70.5211	.955722	.203525	-25.3773	.016307	25.6250	-.020009	.163098	-.369348
0	71.2263	.959053	.218575	-24.9538	.017827	27.5000	-.022123	.175551	-.406332
0	71.9513	.963050	.235079	-24.5876	.019500	29.3750	-.024396	.188567	-.447745
0	72.7635	.967122	.251309	-24.2770	.021130	31.2500	-.026837	.202140	-.488843
0	73.5701	.971467	.267833	-24.0152	.022692	33.1250	-.029448	.216219	-.529008
0	74.3985	.976097	.285447	-23.7970	.024255	35.0000	-.032220	.230779	-.570051
0	75.2467	.981028	.303637	-23.5187	.025810	36.8750	-.035148	.245801	-.611867
0	76.1136	.986065	.321922	-23.4772	.027369	38.7500	-.038237	.261271	-.654810

0	76.9970	.991804	.339733	-23.3630	.024869	40.6250	-.041497	.277164	-.697227
0	77.8943	.997641	.357645	-23.2835	.030253	42.5000	-.044929	.293441	-.737475
0	78.8023	1.003778	.375534	-23.2236	.031525	44.3750	-.048519	.310062	-.775617
0	79.7182	1.010212	.392858	-23.1855	.032691	46.2500	-.052265	.326989	-.811666
0	80.6400	1.016928	.409179	-23.1550	.033739	48.1250	-.056170	.344186	-.845223
0	81.5648	1.023900	.423330	-23.1297	.034597	50.0000	-.060242	.361602	-.873704
0	82.4902	1.031089	.434946	-23.1054	.035266	51.8750	-.064497	.379173	-.896800
0	83.4140	1.038448	.444045	-23.0779	.035774	53.7500	-.068953	.396861	-.915054
0	84.3349	1.045945	.451110	-23.0447	.036175	55.6250	-.073630	.414606	-.930171
0	85.2520	1.053544	.456381	-23.0040	.036494	57.5000	-.078546	.432380	-.942734
0	86.1649	1.061218	.460054	-22.9549	.036742	59.3750	-.083718	.450157	-.953054
0	87.0733	1.068941	.462353	-22.8965	.036927	61.2500	-.089159	.467909	-.961156
0	87.9768	1.076694	.463755	-22.8286	.037077	63.1250	-.094880	.485617	-.968158
0	88.8753	1.084465	.464385	-22.7507	.037187	65.0000	-.100885	.503266	-.973640
0	89.7687	1.092239	.464342	-22.6624	.037263	66.8750	-.107179	.520838	-.977922
0	90.6568	1.100012	.463952	-22.5636	.037331	68.7500	-.113764	.538323	-.981544
0	91.5397	1.107774	.463263	-22.4543	.037376	70.6250	-.120637	.555711	-.984380
0	92.4173	1.115522	.462299	-22.3346	.037413	72.5000	-.127799	.572993	-.986920
0	93.2897	1.123252	.461045	-22.2044	.037436	74.3750	-.135250	.590161	-.988703
0	94.1569	1.130960	.459548	-22.0639	.037453	76.2500	-.142986	.607207	-.990112
0	95.0190	1.138641	.458106	-21.9130	.037465	78.1250	-.151007	.624126	-.991321
0	95.8761	1.146297	.456425	-21.7521	.037473	80.0000	-.159308	.640911	-.992213
0	96.7282	1.153924	.454655	-21.5814	.037478	81.8750	-.167889	.657557	-.992976
0	97.5754	1.161520	.452785	-21.4008	.037483	83.7500	-.176746	.674058	-.993715
0	98.4179	1.169085	.450818	-21.2108	.037485	85.6250	-.185877	.690411	-.994160
0	99.2556	1.176615	.448759	-21.0113	.037485	87.5000	-.195279	.706611	-.994373
0	100.0889	1.184111	.446611	-20.8027	.037486	89.3750	-.204949	.722651	-.994725
0	100.9176	1.191568	.444383	-20.5851	.037486	91.2500	-.214884	.738528	-.995208
0	101.7419	1.198990	.442074	-20.3589	.037485	93.1250	-.225083	.754238	-.995474
0	102.5620	1.206371	.439687	-20.1240	.037484	95.0000	-.235540	.769776	-.995773
0	103.3779	1.213712	.437222	-19.8808	.037483	96.8750	-.246255	.785138	-.995990
0	104.1897	1.221011	.434704	-19.6294	.037483	98.7500	-.257224	.800319	-.996054
0	104.9976	1.228268	.432168	-19.3702	.037490	100.6250	-.268443	.815317	-.995189
0	105.8016	1.235480	.429435	-19.1032	.037489	102.5000	-.279911	.830127	-.995268
0	106.6018	1.242645	.425527	-18.8256	.037481	104.3750	-.291624	.844743	-.996028
0	107.3983	1.249763	.423632	-18.5465	.037476	106.2500	-.303578	.859159	-.996385
0	108.1911	1.256830	.420716	-18.2571	.037474	108.1250	-.315771	.873373	-.996579

PART TWO STEP = 7.499997

REV	THETA	R	PR	PHI	E	TAU	KE9	PXE9
0	108.1911	1.256830	.420716	-18.2571	.037474	108.1250		
0	112.4999	1.294914	.405037	-16.5468	.037610	118.4531		
0	119.9999	1.359307	.376642	-13.0583	.038225	136.9106		
0	127.4999	1.420310	.351933	-9.2404	.039972	155.7594		
0	134.9999	1.478123	.334515	-5.4075	.043794	174.5922		
0	142.4999	1.531225	.311977	-2.0802	.049655	-167.0812		
0	149.9999	1.578041	.282544	.5271	.056113	-149.4734		
0	157.4999	1.618598	.251714	2.5396	.061681	-132.4607		
0	164.9999	1.654005	.224473	4.2075	.065514	-115.7029		
0	172.4999	1.685147	.198819	5.7939	.067365	-99.2163		
0	179.9999	1.713670	.172469	7.5081	.067599	-82.4922		
0	187.4999	1.737013	.145758	9.3738	.069180	-65.6265		
0	194.9999	1.757170	.125484	11.0081	.073038	-48.9521		
0	202.4999	1.774066	.106344	12.4419	.078153	-32.5583		
0	209.9999	1.788471	.099375	13.2886	.084975	-16.7117		
0	217.4999	1.802118	.100491	13.6726	.090803	-1.3276		
0	224.9999	1.815353	.105611	13.7371	.095239	13.7368		

0	232.4999	1.830391	.111497	13.6304	.098126	28.6301
0	239.9999	1.845482	.115669	13.4785	.099697	43.4783
0	247.4999	1.861028	.117856	13.3730	.100375	58.3728
0	254.9999	1.876833	.117932	13.3572	.100676	73.3569
0	262.5000	1.892584	.115374	13.4543	.100749	88.4543
0	270.0000	1.907937	.110145	13.6736	.100724	103.6736
0	277.5000	1.922520	.102400	14.0112	.100705	119.0112
0	285.0000	1.935966	.092195	14.4585	.100708	134.4585
0	292.5000	1.947031	.080170	14.9995	.100810	149.9995
0	300.0000	1.958215	.067231	15.6108	.101069	165.6108
0	307.5000	1.966727	.054877	16.2639	.101556	-178.7361
0	315.0000	1.973724	.046309	16.9150	.102670	-163.0840
0	322.5000	1.980019	.045821	17.5044	.104714	-147.4956
0	330.0000	1.986915	.053858	17.9309	.108664	-132.0691
0	337.5000	1.994143	.052530	18.0630	.114054	-116.9370
0	345.0000	2.000010	.048790	17.9663	.117120	-102.0337
0	352.5000	2.007257	.048538	17.7932	.117833	-87.2068
1	.0000	2.014284	.058916	17.6713	.117495	-72.3287
1	30.0000	2.069582	.125702	16.1900	.141525	-13.8100
1	60.0000	2.133569	.151990	11.5979	.149967	41.6978
1	90.0000	2.221954	.188232	8.8793	.150052	98.8792
1	120.0000	2.325014	.192110	8.5690	.151643	158.5690
1	150.0000	2.420435	.154554	9.5234	.166367	-140.4769
1	180.0000	2.496505	.123194	9.5684	.175887	-80.4319
1	210.0000	2.558670	.113476	9.5953	.192279	-20.1050
1	240.0000	2.634509	.175691	8.7351	.205036	38.7349
1	270.0000	2.737072	.194112	8.9897	.205797	98.9897
1	300.0000	2.828394	.115128	11.4468	.206188	161.4468
1	330.0000	2.858959	-.001353	14.7307	.214550	-135.2693
2	.0000	2.848211	-.022288	16.3997	.222551	-73.6003
2	30.0000	2.837059	-.026176	16.7551	.240605	-13.2449
2	60.0000	2.845063	.028200	14.6196	.251157	44.6196
2	90.0000	2.865175	.053872	12.4042	.251355	102.4041
2	120.0000	2.907873	.113553	10.7760	.252407	160.7760
2	150.0000	2.979355	.149458	9.7290	.262958	-140.2713
2	180.0000	3.062206	.156958	8.3638	.276553	-81.6165
2	210.0000	3.137173	.140556	7.7043	.293742	-22.2959
2	240.0000	3.232488	.226718	6.5640	.305316	36.5637
2	270.0000	3.370347	.261953	7.3281	.305756	97.3281
2	300.0000	3.490237	.134576	10.5393	.306012	160.5393
2	330.0000	3.511529	-.048419	14.7137	.313369	-135.2803
3	.0000	3.470400	-.074096	17.3543	.322457	-72.6457
3	30.0000	3.436225	-.045294	18.4179	.343205	-11.5821
3	60.0000	3.418933	-.035032	17.1937	.352884	47.1937
3	90.0000	3.397698	-.033015	15.4215	.353028	105.4215
3	120.0000	3.403377	.070454	13.4270	.353694	163.4269
3	150.0000	3.470403	.171395	11.7275	.366066	-138.2729
3	180.0000	3.557031	.173509	10.1553	.377295	-79.8450
3	210.0000	3.646434	.142106	9.3511	.396823	-20.6422
3	240.0000	3.747132	.254210	8.4528	.407358	38.3425
3	270.0000	3.911535	.316940	9.3838	.407637	99.3838
3	300.0000	4.052300	.139346	12.9634	.407824	162.9634
3	330.0000	4.055265	-.104831	17.4602	.414174	-132.5398
4	.0000	3.952543	-.117244	20.3535	.423032	-69.6465
4	30.0000	3.934705	-.056103	21.5243	.446352	-8.4757
4	60.0000	3.907154	-.073339	20.6357	.455712	50.6357
4	90.0000	3.856167	-.098391	19.0304	.455804	109.0303
4	120.0000	3.837973	.051771	16.7678	.456251	166.7678
4	150.0000	3.910259	.205832	14.7104	.467406	-135.2900

4	180.0000	4.023921	.197081	13.1630	.473551	-76.8352
4	210.0000	4.103974	.131371	12.4402	.500655	-17.5601
4	240.0000	4.204304	.271717	11.5725	.510327	41.5723
4	270.0000	4.369357	.365531	12.7500	.510464	102.7500
4	300.0000	4.549343	.135846	16.6535	.510597	166.5535
4	330.0000	4.525527	-.173667	21.1753	.516079	-128.8247
5	.0000	4.422070	-.158296	24.0659	.523781	-65.9341
5	30.0000	4.355822	-.052572	25.1150	.550573	-4.8850
5	60.0000	4.335995	-.096571	24.3368	.558544	54.3368
5	90.0000	4.261992	-.152036	22.7890	.558585	112.7889
5	120.0000	4.225513	.044201	20.3163	.558898	170.3162
5	150.0000	4.310366	.254936	18.0396	.568825	-131.9608
5	180.0000	4.446583	.218455	16.6670	.579324	-73.3333
5	210.0000	4.523836	.110688	16.1746	.603915	-13.8257
5	240.0000	4.619470	.280949	15.5032	.612738	45.5029
5	270.0000	4.823147	.414599	16.8398	.612822	106.8398
5	300.0000	4.997401	.124199	20.8457	.612846	170.8457

PART THREE

REV	THETA	R	PR	PHI	Ė	TAU	XE9	PXE9
5	270.0000	4.823147	.414599	16.8398	.612822	106.8398		
6	.0000	4.802786	-.202813	28.4911	.623510	-61.5089		
6	180.0000	4.848062	.237657	20.8228	.676060	-59.1775		
7	.0000	5.117205	-.230231	32.3930	.720261	-57.6070		

STOP 0